STRAIN BASED SELECTION OF FRICTION ANGLE FOR GEOTECHNICAL DESIGN

by

Emirhan Sancak

B.S., Civil Engineering, Yıldız Technical University, 2011

Submitted to the Institute for Graduate Studies in
Science and Engineering in partial fulfillment of
the requirements for the degree of
Master of Science

Graduate Program in Civil Engineering

Boğaziçi University

2014

STRAIN BASED SELECTION OF FRICTION ANGLE FOR GEOTECHNICAL DESIGN

APPROVED BY:

Assoc. Prof. Özer Çinicioğlu (Thesis Supervisor)	.....
Prof. Erol Güler	.....
Assoc. Prof. Pelin Tohumcu Özener	.....

DATE OF APPROVAL: 12 August 2014

ACKNOWLEDGEMENTS

First of all, I would like to express my sincere thanks to my thesis supervisor Associate Prof. Özer Çinicioğlu. I am extremely grateful and indebted to him for his expert, valuable guidance and encouragement extended to me throughout my study.

I place on record, my sincere gratitude to the member of the thesis committee, Prof. Erol Güler and Associate Prof. Pelin Tohumcu Özener for their efficient comments.

I also thank to my friends, Behzad Soltanbeigi, Ahmet Talha Gezgin, Emrah Kılıç, Cihan Cengiz for their help and patience during my study.

Last but not the least; I take this opportunity to record my sincere thanks to my family for their encouragement and standing by me in whole of my life.

Finally, I would like to express my gratitude to The Scientific and Technological Research Council of Turkey (TUBİTAK) for supporting this research through Project number 110M595.

ABSTRACT

STRAIN BASED SELECTION OF FRICTION ANGLE FOR GEOTECHNICAL DESIGN

When it comes to make a decision on selecting a design friction angle for geotechnical engineering applications, engineers either prefer to use peak friction angle accepting a smaller factor of safety or use the critical state friction angle as a design friction angle by neglecting the rewarding effects of dilatancy. However, in a project if it is predicted that the soil would not reach failure at any point within the geotechnical structure, then choosing peak friction angle as the design friction angle would be beneficial in terms of economy. Starting from this point, the goal in this study is to develop a method that would guide the engineer in the selection of an appropriate soil friction angle. For this purpose, it is attempted to quantify shear strain at failure as a function of soil properties. Towards this goal, triaxial data of 8 different sands were investigated. These data was used to construct relationships between peak dilatancy angle (ψ_p) and shear strain (ε_q) at which these peak dilatancy angles are measured. The reason for choosing this relationship is the inherent link between failure and peak dilatancy; peak dilatancy is always measured at the instance of maximum shear stress. Later, obtained ψ_p-ε_q functions for all sands are plotted on the same graph. This graph revealed that ψ_p-ε_q functions are dependent on the mean grain diameter (D_{50}). As a result, a new method for assessing the shear strain limit for using peak friction angle as the design friction angle is proposed. This method uses D_{50} as input and calculates magnitude of shear strain at failure as a function of ψ_p. Combining this method with the equation proposed by Çinicioğlu *et al.*, (2013) that calculates ψ_p as a function of in-situ stress and density of soil, it becomes possible to calculate shear strain at failure magnitude from the knowledge of in-situ stress, density and D_{50} values.

ÖZET

GEOTEKNİK TASARIMLARDA İÇSEL SÜRTÜNME AÇISININ GERİNİM ESASLI SEÇİMİ

Geoteknik mühendislik uygulamarında tasarım içsel sürtünme açısının belirlenmesi noktasında, mühendisler ya küçük bir emniyet katsayısı ile birlikte tepe içsel sürtünme açısını ya da genleşim açısının faydalı etkisini yok sayarak kritik durum içsel sürtünme katsayısını tercih etmektedirler. Ancak, bir projede eğer geoteknik yapının hiçbir yerinde zemin göçme durumuna ulaşmayacaksa, tasarım esnasında tepe sürtünme açısının kullanılması ekonomik açıdan yarar sağlayacaktır. Buradan yola çıkarak, bu çalışmanın amacı, uygun bir içsel sürtünme açısının belirlenmesinde mühen dislere yol gösterecek bir yöntem geliştirmektir. Bu doğrultuda, zemin özelliklerinin bir fonksyonu olarak göçme anındaki kayma geriniminin ölçülmesine çalışılmıştır. Bu amaçla, sekiz farklı kuma ait üç eksenli deney verileri incelenmiştir. Bu veriler, tepe genleşim açıları (ψ_p) ile ölçülen bu tepe genleşim açılarına denk gelen kesme gerinimleri (ε_q) arasında ilişki kurmak üzere kullanılmıştır. Bu ilişkinin seçilmesinin sebebi, göçme ile tepe genleşim açısı arasında tepe genleşim açısının her zaman maksimum kesme geriliminin var olması durumunda ölçülmesi gibi doğal bir ilişkinin varolmasıdır. Tüm kumlar için elde edilen ψ_p-ε_q fonksyonları aynı grafik üzerinde gösterilmiştir. Bu grafik ψ_p-ε_q fonksiyonlarının ortalama tanecik çapı (D_{50})'na bağlı olduğunu ortaya koymuştur. Sonuç olarak, tepe içsel sürtünme açısını tasarım içsel sürtünme açısı olarak kullanmak için kesme gerinim limitini degerlendirmek üzere yeni bir yöntem sunuldu. Bu yöntemle D_{50} girdi olarak kullanılarak kesme gerinimini tepe genleşim açısının bir fonksiyonu olarak hesaplanabilmektedir. Bu yöntem ile Çinicioğlu v.d. (2012) tarafından sunulan, yerinde gerilime ve zemin yoğunluğuna bağlı olarak tepe genleşim açısını hesaplayan denklem birleştirildiğinde göçme durumundaki kesme gerinimini yerinde gerilim, zemin yoğunluğu ve D_{50} değerlerinin bilgisiyle hesaplamak mümkün olmaktadır.

TABLE OF CONTENTS

ACKNOWLEDGEMENTS . . . iii
ABSTRACT . . . iv
ÖZET . . . v
LIST OF FIGURES . . . viii
LIST OF TABLES . . . xiii
LIST OF SYMBOLS . . . xv
LIST OF ACRONYMS/ABBREVIATIONS . . . xviii
1. INTRODUCTION . . . 1
1.1. Theory Background . . . 1
2. LITERATURE REVIEW . . . 3
2.1. Shear Strength and Dilatancy Properties of Soils . . . 3
2.1.1. An Introduction to Peak Friction Angle and Dilatancy Angle of Cohesionless Soils . . . 3
2.1.2. Taylor's Theory . . . 8
2.1.3. Rowe's Theory . . . 10
2.1.4. Bolton's Equation . . . 11
2.1.5. Schanz and Vermeer Equation . . . 14
2.1.6. Vaid and Sasitharan Equation . . . 16
2.1.7. Cinicioglu and Abadkon Equation . . . 19
3. METHODOLOGY FOR THE TESTING OF ANALYZED SANDS . . . 20
3.1. K_0 Triaxial Testing Program . . . 20
3.2. Testing Material . . . 23
3.2.1. Silivri Sand . . . 23
3.2.2. Erksak Sand . . . 24
3.2.3. Anatolian Sands . . . 25
3.3. Sample Preparation . . . 26
3.4. Automatic Triaxial Testing Apparatus . . . 28
3.5. Triaxial Testing Procedure . . . 29
3.5.1. Initialization Phase . . . 29

3.5.2. Saturation Phase 30
3.5.3. Consolidation Phase 30
3.5.4. Shearing Phase 31
3.6. Triaxial Test Corrections 31
3.6.1. Piston Area Correction 31
3.6.2. Correction for the Rubber Membrane 33
3.6.3. Correction for Sample Area 35
4. EVALUATION OF TRIAXIAL TEST RESULTS 38
4.1. Results of the Triaxial Tests with Silivri Sand 38
4.2. Results of the Triaxial Tests with Erksak Sand 42
4.3. Results of the Triaxial Tests with Anatolia Sands 43
5. DISCUSSION 53
5.1. Effect of Soil Properties on Peak Dilatancy Angle-Shear Strain at Failure Relationships 53
5.2. Effect OCR on Peak Dilatancy Angle-Shear Strain at Failure Relationship 57
5.3. Implementation of this Method to Design 59
5.3.1. Example 1: Strain-Based Selection of Design Friction Angle According to Results of a FEM Software 61
5.3.2. Example 2: Strain-Based Selection of Design Friction Angle According to Results of Retaining Wall Physical Model Experiments 65
6. CONCLUSION 70
REFERENCES 72

LIST OF FIGURES

Figure 2.1. Mohr Circle. 3

Figure 2.2. Stress-Strain Curve Representing Peak Angle Critical State Friction Angle. 4

Figure 2.3. Dilative Behavior. 5

Figure 2.4. Stress-Strain Relationship up to Residual Strength. 6

Figure 2.5. Sawtooth Model. 7

Figure 2.6. Sliding Blocks. 7

Figure 2.7. Taylor's Energy Dissipation Analogy. 9

Figure 2.8. Rowe's Sliding Mechanism. 11

Figure 2.9. Comparison of Bolton's Data with Rowe's and Taylor's. 12

Figure 2.10. Variation of Dilatancy Angle with Relative Density. 13

Figure 2.11. Sliding Mechanisms Presented. 14

Figure 2.12. Stress Paths Applied. 16

Figure 2.13. Relationship Between Peak Friction Angle and Maximum Dilatancy Rate. 17

Figure 2.14. ϕ'_{peak}-ψ_{max} Plot in Terms of Both Triaxial Compression and Extension Tests. 19

Figure 3.1. Grain Size Distribution of Silivri Sand. 23

Figure 3.2. Vibratory Table Used to Determine Maximum Minimum Void Ratios. 24

Figure 3.3. The Grain Size Distribution of Erksak Sand Used in Sasitharan's Study. 25

Figure 3.4. Air-Pluviation Set-Up. 27

Figure 3.5. Variation of Void Ratios of Samples with Raining Height. 27

Figure 3.6. Automatic Triaxial Testing Apparatus. 28

Figure 3.7. Schematic of a Flow Trac Unit. 29

Figure 3.8. Piston Area Correction Test. 32

Figure 3.9. Variation of Uplift Force with Cell Pressure. 33

Figure 3.10. Tensile Test. 34

Figure 3.11. None Area Correction. 35

Figure 3.12. Uniform Area Correction. 35

Figure 3.13. Parabolic Area Correction. 36

Figure 3.14. Parabolic Shape of the Sample During Shearing. 37

Figure 4.1. Peak Dilatancy Angle-Shear Strain at Failure Response Based on the Triaxial Experiments Over Silivri Sand. 41

Figure 4.2. Variation of Peak Dilatancy Angle With Shear Strain at Failure for Erksak Sand. 43

Figure 4.3. Peak Dilatancy Angle-Shear Strain at Failure Response of Specimen A. 47

Figure 4.4. Peak Dilatancy Angle-Shear Strain at Failure Response of Specimen B. 48

Figure 4.5. Peak Dilatancy Angle-Shear Strain at Failure Response of Specimen C. 48

Figure 4.6. Peak Dilatancy Angle-Shear Strain at Failure Response of Specimen D. 49

Figure 4.7. Peak Dilatancy Angle-Shear Strain at Failure Response of Specimen E. 49

Figure 4.8. Peak Dilatancy Angle-Shear Strain at Failure Response of Specimen F. 50

Figure 5.1. Variation of α With Median Grain Size, D_{50}. 54

Figure 5.2. Variation of β With Median Grain Size, D_{50}. 55

Figure 5.3. Variation of Shear Strain at Failure With Peak Dilatancy Angle and Median Grain Size. 56

Figure 5.4. Peak Dilatancy Angle-Shear Strain at Failure Response in Case of OCR=1. 57

Figure 5.5. Peak Dilatancy Angle-Shear Strain at Failure Response in Case of OCR=2. 57

Figure 5.6. Peak Dilatancy Angle-Shear Strain at Failure Response in Case of OCR=4. 58

Figure 5.7. Peak Dilatancy Angle-Shear Strain at Failure Response in Case of OCR=8. 58

Figure 5.8. Total Displacements in y Direction as a Result of 0.1 M Vertical Displacement of the Structure. 62

Figure 5.9. Total Shear Strains as a Result of 0.1 M Vertical Displacement of the Structure. 62

Figure 5.10. Determining the Shear Strain at Failure Value of Silivri Sand With a D_{50} Value of 0.365 by the Proposed Method. 63

Figure 5.11. Total Displacements in y Direction as a Result of 2 cm Vertical Displacement of the Structure. 64

Figure 5.12. Total Shear Strains as a Result of 2 cm Vertical Displacement of the Structure. 64

Figure 5.13. Experimental Set-Up. 65

Figure 5.14. Typical Results of PIV Method. 66

Figure 5.15. Shear Band Formation with Respect to Wall Movement. 67

Figure 5.16. Determining the Shear Strain at Failure Value of Akpinar Sand with a D_{50} value of 0.365 by the Proposed Method. 68

Figure 5.17. Shear Band Formations With Respect to Lesser Diplacements. . . 69

LIST OF TABLES

Table 3.1. Experimental Program. 21

Table 3.2. Main Properties of the Sand Used in this Study. 24

Table 3.3. Main Properties of the Sand Used in this Study. 25

Table 3.4. Locations of Samples Used in the Study 26

Table 3.5. Main Properties of Sands Used. 26

Table 4.1. Data Obtained From the Experiments Over Standard Ottawa Sand. 39

Table 4.2. Data Obtained From the Experiments Over Standard Ottawa Sand (Cont.). 40

Table 4.3. Summary of the Data Obtained From. 42

Table 4.4. Results of Experiments Conducted with Specimens of A. 44

Table 4.5. Results of Experiments Conducted with Specimens of B. 44

Table 4.6. Results of Experiments Conducted with Specimens of C. 45

Table 4.7. Results of Experiments Conducted with Specimens of D. 45

Table 4.8. Results of Experiments Conducted with Specimens of E. 46

Table 4.9. Results of Experiments Conducted with Specimens of F. 47

Table 5.1. Properties of the Sands Investigated in This Study. 54

Table 5.2. Properties of Akpinar and Silivri Sands. 62

LIST OF SYMBOLS

A_c	Corrected area of the sample
A_0	Initial area of the sample
A_m	Area of the membrane
B	Pore pressure parameter
C_{comp}	Compression index of the soil
C_u	Coefficient of uniformity
C_c	Coefficient of curvature
D_R	Relative density
D_{50}	Median grain size
E_m	Young's modulus for the membrane material
e_{min}	Minimum void ratio
e_{max}	Maximum void ratio
e	Void ratio
F_b	Buoyancy force
h	Sand raining height
h_c	Height of sample after consolidation
h_0	Initial height of the sample
I_D	Density index
I_R	Relative density index
K	Coefficient of the internal friction
L	Unstretched length of the membrane
P'_A	Atmospheric pressure
p'	Mean effective stres
Q	Constant value for Bolton relative density equation
q	Deviatoric stress
r	Constant parameter showing the amount of dilatancy contribution to shear strength property of soil
t_m	Membrane thickness
V_c	Volume of the sample after consolidation phase

W	Work input
W_s	Width of circumferential strip
α	Angle of shearing in sawtooth plane
α	Fitting parameter depending on D_{50}
a_ψ	Slope of line correlating dilatancy angle with mean effective stress and relative density
β	Angle of sliding on sawtooth plane
β	Fitting parameter depending on D_{50}
$d\varepsilon_v$	Volumetric strain change
$d\varepsilon_q$	Deviatoric strain change
Δu	Pore pressure change
ΔL	Change in length of the membrane
Δh	Change in height of the specimen
εa	Axial strain
εq	Shear strain
$\varepsilon q - f$	Shear strain at failure
εr	Radial strain
εv	Volumetric strain
$\dot{\varepsilon}_1$	Strain rate in vertical direction
$\dot{\varepsilon}_2$	Strain rate in horizontal direction
$\dot{\varepsilon}_3$	Strain rate in horizontal direction
$\dot{\varepsilon}_\nu$	Volumetric strain rate
$\dot{\varepsilon}$	Shearing strain rate for triaxial test
ϕ'	Friction angle
λ	Ratio of the effective horizontal stress change to effective vertical stress change
m_ψ	Fitting parameter varying with relative density index I_D
ϕ'_c	Critical state friction angle
σ'_{1f}	Effective vertical stress at failure
σ'_{3f}	Effective horizontal stress at failure
σ'_c	Effective confining pressure

σ'_n	Effective normal stress
ψ	Dilatancy angle
ψ_p	Peak dilatancy angle
ρ	Shear stress

LIST OF ACRONYMS/ABBREVIATIONS

ASTM	American society for testing and materials
CD	Consolidated drained
FEM	Finite element method
OCR	Overconsolidation ratio
PIV	Particle image velocimetry

1. INTRODUCTION

1.1. Theory Background

Friction angle for cohesionless soils is acknowledged as the only shear strength parameter. Basically, two versions of friction angles are used by geotechnical engineers; peak friction angle and critical state friction angle. Peak friction angle is expressed by Bishop (1950) in terms of critical state friction angle and peak dilatancy. By decades, many researchers studied on that parameter. In the light of Rowe's (1962) well-established theory pertaining stress and strain ratio, Bolton (1986) rearranged the relationship between the peak friction angle, ϕ'_p, and the critical state friction angle, ϕ'_c, with a consideration of dilatant behavior.

It is clearly seen that one of the most frequently faced problem within geotechnical engineering applications in practice is the selection of an appropriate value for the friction angle to be used for design. Mostly, the critical state friction angle is preferred as design friction angle omitting the effect of dilatancy by practitioners in order to be on the safe side. Because the peak strength, at which the peak friction angle is mobilized, depends on the density and the stress state of the soil mass. As a result, ϕ'_p is not a soil constant, and is unlikely to be the same throughout the mass of soil. Besides, it is unlikely that the peak strength will be mobilized simultaneously throughout the soil mass; instead, progressive failure at an average strength rather lower than the peak may occur (Powrie, 2004). However, the factors of safety used in many traditional methods of design may well allow for these possibilities, and their use in connection with the critical state strength could lead to overconservatism which may result with economical losses.

Starting from this point of view, the aim of this study is to present an alternative way, based on deformation and strain limits of structures that will aid engineers in the selection of design friction angles.

For this purpose, firstly an extensive literature review regarding shear strength parameters of cohesionless soils was held. Afterwards, a bulk of triaxial compression test data under drained condition produced by previous researchers in Bogazici University Geotechnical Laboratory was analyzed and the results were used to develop a relationship between ψ_p and ε_q at failure (ε_{q-f}). Later, forms of ψ_p-ε_{q-f} relationships for different sands available in literature have been examined. Finally, all data were used to construct a method that would yield ε_{q-f} as a function of soil's in-situ stress state, density, and mean grain diameter (D_{50}). Developed methods are used on the physical retaining model test data and the results are discussed.

2. LITERATURE REVIEW

This literature review summarizes the developments on our understanding of shear strength and dilatancy in case of cohesionless soils.

2.1. Shear Strength and Dilatancy Properties of Soils

Researches and theories about shear strength and dilatancy of cohesionless soils are reviewed in brief within this chapter.

2.1.1. An Introduction to Peak Friction Angle and Dilatancy Angle of Cohesionless Soils

Peak friction angle is defined as the maximum friction angle possessed by the soil when it reaches its maximum shear strength. Using Mohr Circle is rather practical way to obtain peak friction angle at failure:

$$sin\phi = \frac{\sigma'_{1f} - \sigma'_{3f}}{\sigma'_{1f} + \sigma'_{3f}} \tag{2.1}$$

where ϕ' is friction angle, σ'_{1f} is major principle stress at failure, σ'_{3f} is minor principle stress at failure.

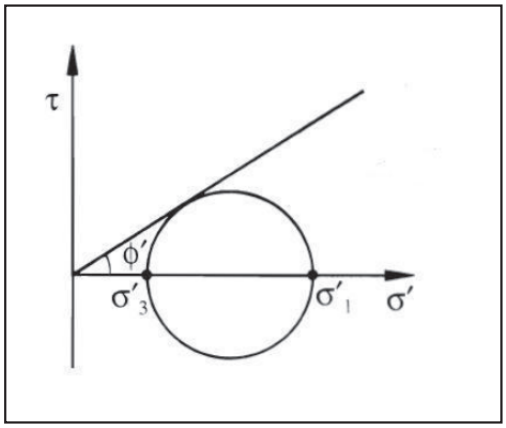


Figure 2.1. Mohr Circle.

The other friction angle is the so called critical state friction angle. Critical state is referred to the state during which the soil is sheared at constant volume and constant rate. Critical state friction angle is the friction angle that defines the frictional characteristics of the soil at the critical state. In other words, the soil under shearing attains to the critical state when shear stress being applied on the soil become steady where shear strain still increasing. Notation of the critical state friction angle is ϕ'_c. Critical state friction angle is one of major soil parameter, which is also dependent on only the mineralogy of the soil. For that reason, Critical state friction angle is taken into account as a constant for a soil.

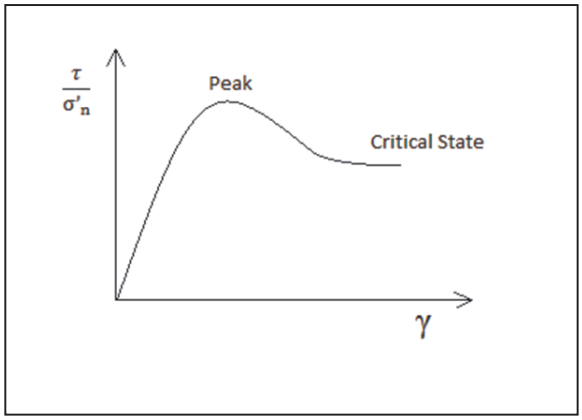


Figure 2.2. Stress-Strain Curve Representing Peak Angle Critical State Friction Angle.

When compacted granular soils are sheared, an expansion in volume is observed as a result of that the grains without any freedom to move start to slide over each other. Theoretically, dilatancy is defined as the volume change during shearing. The rate of dilation is mathematically defined as:

$$sin\psi = \frac{d\varepsilon_v}{d\varepsilon_q} \tag{2.2}$$

Where ψ is notation of dilatancy angle, $d\varepsilon_\nu$ is volumetric strain change, $d\varepsilon_q$ is shear strain change. When it comes to define dilatancy angle in terms of triaxial tests, the

formula above can be derived as:

$$sin\psi = \frac{-(\dot{\varepsilon}_1 + \dot{\varepsilon}_2 + \dot{\varepsilon}_3)}{\dot{\varepsilon}_1 - \dot{\varepsilon}_3} \tag{2.3}$$

where ψ is dilatancy angle, $\dot{\varepsilon}_1$ is the vertical strain rate, $\dot{\varepsilon}_2$ and $\dot{\varepsilon}_3$ are horizontal strain rates which are on two different direction perpendicular to each other. The equation can be rewritten in terms of plane-strain conditions considering $\dot{\varepsilon}_2 = 0$:

$$sin\psi = \frac{-(\dot{\varepsilon}_1 + \dot{\varepsilon}_3)}{\dot{\varepsilon}_1 - \dot{\varepsilon}_3} \tag{2.4}$$

During shearing, depending on the initial density, the soil either expands or compresses. Dilatancy angles corresponding to these states are positive and negative, respectively. This is contrary to the general sign notation in soil mechanics where compression is considered to be positive.

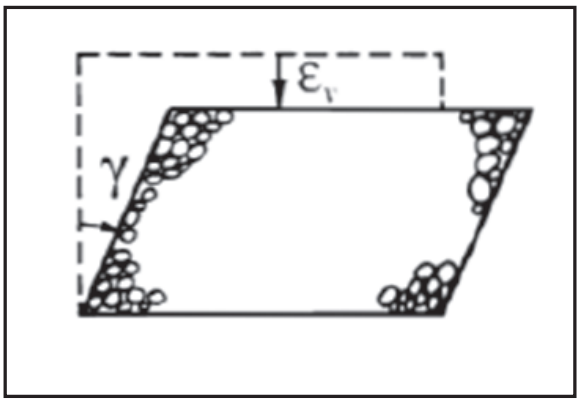


Figure 2.3. Dilative Behavior.

When a soil of loose sand is sheared, principal stress difference that corresponds to shear stress does not show peak behavior. As a result, principal stress difference reaches its maximum value gradually. Thus, positive dilation (volume increase due to shearing) is non-existent among loose sands. The friction angle for these loose soils is always equal to critical state friction angle.

Generally, critical state friction angle is a lower bound to the friction angle.

However, there is an exception to this rule if the soils contain sufficient amount of clays. These types of soils which contain large amounts of plate-like particles such as clays, have even smaller friction angles if they are sheared to large-enough strains. This friction angle is called residual friction angle.

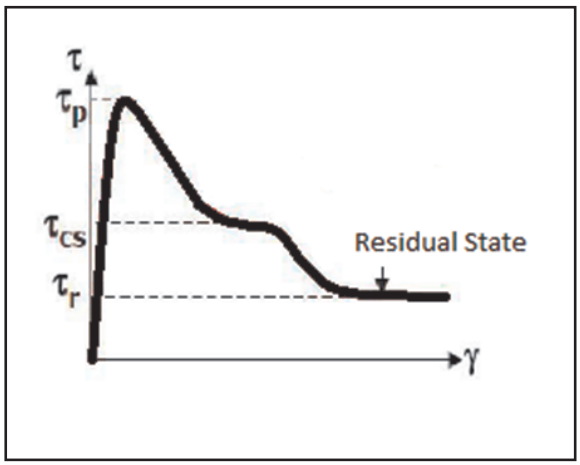


Figure 2.4. Stress-Strain Relationship up to Residual Strength.

Unlike loose sands, dense sands show peak strength before reaching the critical state. Overcoming the interlocked arrangement between densely arranged soil grains, the peak strength is mobilized by overcoming dilatancy effect. Therefore, it can be proposed that peak friction angle is the sum of the effects of critical state friction angle and dilatancy angle.

In light of the above information, it is understood that dilatant behavior is responsible for the difference between peak and critical state friction angles. A successful educational analogy proposed by Taylor (1948) to explain the influence of dilatancy on peak strength is the sawtooth model.

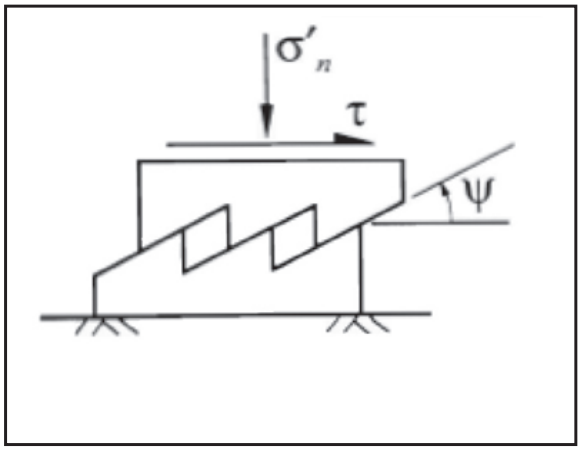


Figure 2.5. Sawtooth Model (Houlsby, 1991).

In Figure 2.6, a normal stress "σ'_n" and a shear stress "τ" are applied to frictional blocks. There is friction on the surface between two blocks which can be regarded as "ϕ'_c". So that:

$$\frac{\tau}{\sigma_n} = tan\phi'_c \tag{2.5}$$

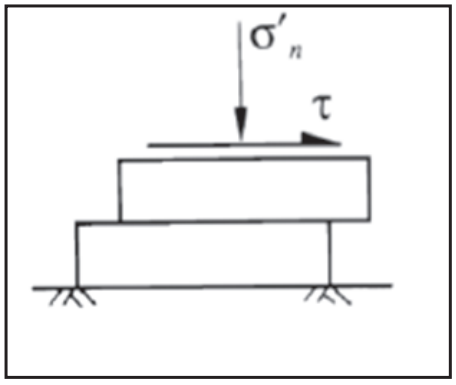


Figure 2.6. Sliding Blocks.

If the surface between two blocks above in Figure 2.6 is like a sawtooth which has teeth with an angle "ψ", it would be an addition to the friction angle "ϕ'_c" already

acting on the plane, thus the relationship between ϕ' and ϕ'_c can be defined as:

$$\frac{\tau}{\sigma_n} = tan\phi' = \tan\left(\phi'_c + \psi\right) \tag{2.6}$$

Hence the friction angle can be derived as:

$$\phi' = \phi'_c + \psi \tag{2.7}$$

Hereby summation of critical state friction angle and dilatancy angle equals to the peak friction angle. Numerous theories, some of which is discussed below, are established in order to state the relationship between friction angles.

2.1.2. Taylor's Theory

The relationship between dilatancy and friction angles was investigated in Taylor's research. It was one of the first studies on the topic. His research is mainly based on the dissipation of work due to friction between soil grains. In other words, entire friction formation in soils is described in terms of energy dissipation. He derived the equation below by utilizing the sliding block on an even surface:

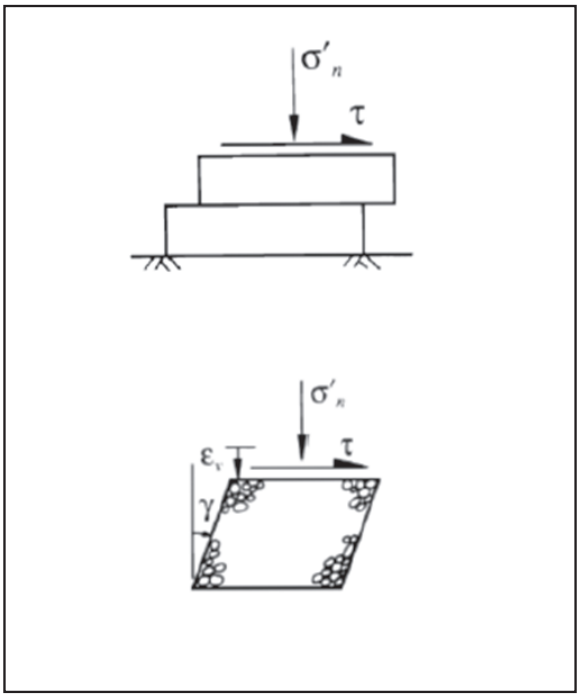


Figure 2.7. Taylor's Energy Dissipation Analogy (Taylor, 1948).

$$W = \tau\gamma \tag{2.8}$$

where W represents rate of work and γ is the shear strain. The Equation 2.8 can be written as below in terms of the normal stress and shear strain rate:

$$W = (tan\phi'_c)\,\sigma_n\gamma \tag{2.9}$$

where $tan\phi'_c$ represents the constant of proportionality between the work dissipated and the stress-strain couple. But Taylor, in his work, put $\sigma'_n\varepsilon'_v$ as a work input in order to emphasize dilation where σ'_n conducts work instead of τ:

$$W = (tan\phi'_c)\,\sigma_n\gamma = \sigma'_n\dot{\varepsilon}_v + \tau\gamma \tag{2.10}$$

Afterwards, with regards to previous information, Equation 2.11 is obtained by putting $\frac{\tau}{\sigma'_n} = tan\phi'$ and $tan\psi = -\frac{\dot{\varepsilon}_v}{\gamma}$ in charge:

$$tan\phi' = tan\phi'_{cv} + tan\psi \tag{2.11}$$

The equation obtained above differs from that obtained by sawtooth model. However it justifies that the friction angle is a function of critical state friction angle and dilatancy angle.

2.1.3. Rowe's Theory

The concept that Rowe used in his work (1962) differs from which is used in Taylor's work. However both Taylor and Rowe obtained fairly similar results. Rowe's approach is mainly based on assemblies of grains in a geometrical aspect. He put forward expressions in order to define stress ratio and strain rate ratio. Rowe considers the sliding surface as the sawtooth model where α and β angles are used to obtain stress and strain ratios. The Equation 2.12 is arranged as seen below by eliminating α:

$$\frac{\sigma'_1}{\sigma'_3} = \frac{tan\left(\phi'_\mu + \beta\right)}{tan\beta} \frac{-\dot{\varepsilon}_3}{\dot{\varepsilon}_1} \tag{2.12}$$

where ϕ'_μ represents the fundamental friction angle for grain to grain contact. According to minimum energy hypothesis, Rowe obtained β angle as "$\frac{\pi}{4} - \frac{\phi'_\mu}{2}$". In brief the hypothesis of minimum energy indicates that the energy ratio shows differences due to particle formation. The equation is rearranged as:

$$\frac{\sigma'_1}{\sigma'_3} = tan^2\left(\frac{\pi}{4} - \frac{\phi'_\mu}{2}\right)\left(\frac{-\dot{\varepsilon}_3}{\dot{\varepsilon}_1}\right) \tag{2.13}$$

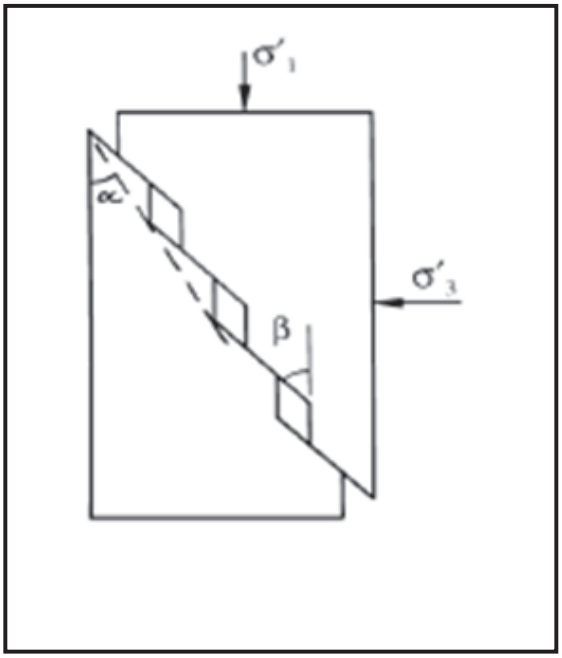


Figure 2.8. Rowe's Sliding Mechanism (Rowe, 1962).

Short form of the Equation 2.13 can simply be arranged as:

$$R = KD \tag{2.14}$$

where R represents stress ratio, K is internal friction coefficient and D is strain ratio. K is derived as:

$$K = tan^2\left(45 + \frac{\phi_f}{2}\right) \tag{2.15}$$

2.1.4. Bolton's Equation

The scope of Bolton's work (1986) includes plain strain tests and the comparison of his data with 17 different sands. Bolton compared his findings with Taylor's and Rowe's theories and revealed that there is a smooth correlation between them.

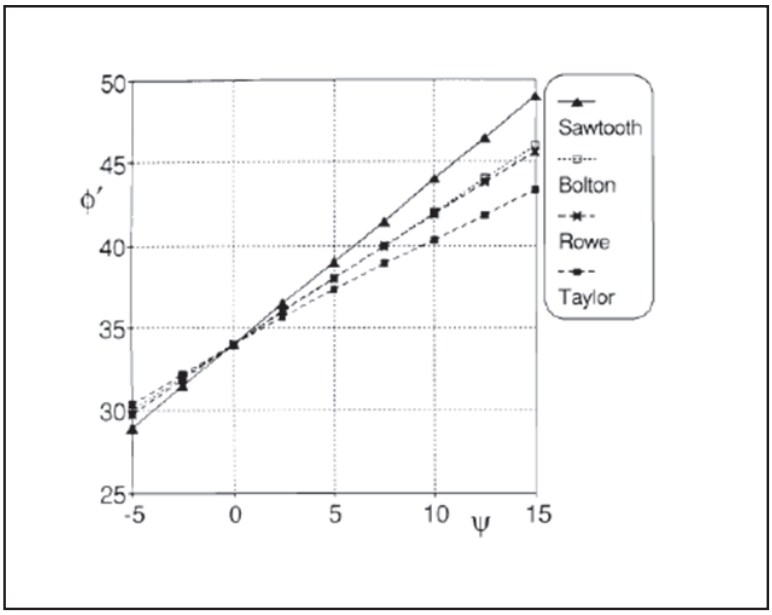


Figure 2.9. Comparison of Bolton's Data with Rowe's and Taylor's (Bolton, 1986).

As observed in Figure 2.9, Bolton brought forward an empirical equation which corresponds with Taylor's equation and the Rowe's considerably. He defined a new behavior of soil of sand in terms of relative density. Based on the data which was obtained as a result of experiments conducted on numerous sand samples, Bolton proposed the Equation 2.16 below:

$$\phi'_{peak} = \phi'_c + 0.8\psi \tag{2.16}$$

where ϕ'_{peak} represents the peak friction angle, ϕ'_c is the critical state friction angle and ψ is the dilatancy angle. In the light of the data Bolton (1986) obtained, following equations regarding relative density were proposed.

In terms of plain strain test:

$$\phi'_{max} - \phi'_{cv} = 0.8\psi = 5I_R \tag{2.17}$$

In terms of triaxial test:

$$\phi'_{max} - \phi'_{cv} = 0.8\psi = 3I_R \tag{2.18}$$

where I_R represents relative density index. I_R is obtained from:

$$I_R = I_D\,(Q - lnp') - R \tag{2.19}$$

where I_D is density index of soil, Q and R are constants which Bolton identified to be 10 and 1, respectively. Thus the Equation 2.19 can be rearranged as:

$$I_R = I_D\,(10 - lnp') - 1 \tag{2.20}$$

With respect to the equations Bolton (1986) obtained, the relationship between dilatancy angle and relative density can be clearly seen in the figure below:

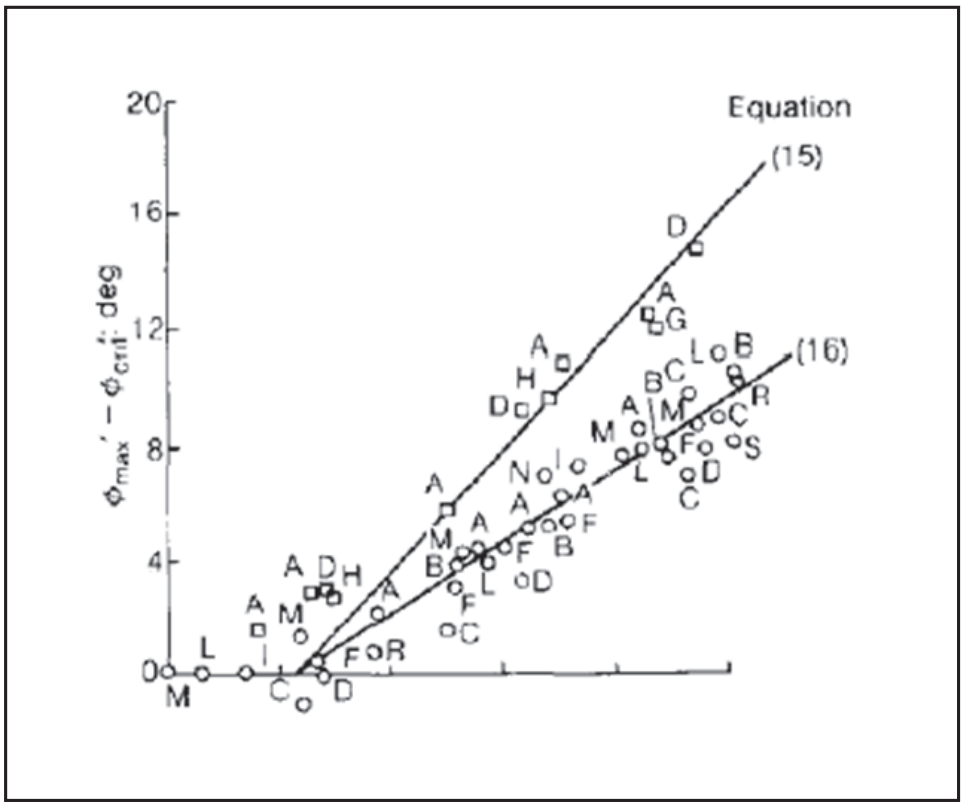


Figure 2.10. Variation of Dilatancy Angle with Relative Density (Bolton, 1986).

The zero dilatancy corresponds to relative density with a value of 0.23 in Figure 2.10. Bolton also regards dilatancy angle as an ineffective parameter in terms of triaxial compression test, so that mean strains in vertical planes are contractile. Therefore he suggested applying $\left(- \frac{d\varepsilon_v}{d\varepsilon_1} \right) max$ in order to obtain dilatancy rate in triaxial test. Bolton (1986) proposed following equation for both triaxial and plane strain tests:

$$\left(-\frac{d\varepsilon_v}{d\varepsilon_1} \right) \max = 0.3 I_R \tag{2.21}$$

2.1.5. Schanz and Vermeer Equation

Schanz and Vermeer (1996) examined the dilatancy angle provided by plane-strain and triaxial tests they conducted within their work. They obtained the dilatancy angle in terms of biaxial state. In Figure 2.11, 2 planes, which are σ_1 - σ_2 and σ_1 - σ_3, are shown and represented by A and B sliding mechanisms. These sliding mechanisms occur as a result of planary deformation.

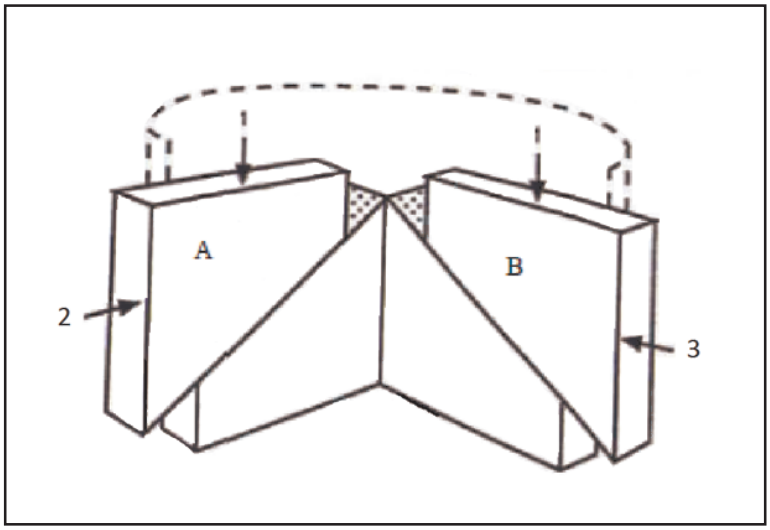


Figure 2.11. Sliding Mechanisms Presented by (Schanz, 1995).

Based on the sliding mechanism formula, Schanz and Vermeer derived following

formulas for each mechanism:

$$\left(\frac{-\dot{\varepsilon}_2}{\dot{\varepsilon}_1}\right) A = D_A = \frac{R_A}{K} \tag{2.22}$$

$$\left(\frac{-\dot{\varepsilon}_3}{\dot{\varepsilon}_1}\right) B = D_A = \frac{R_B}{K} \tag{2.23}$$

where $R_A = R_B = R$ and $\dot{\varepsilon}_3$=$\dot{\varepsilon}_2$ due to triaxial test conditions. In addition to this, the axial strain rate can be interpreted as:

$$\dot{\varepsilon}_1 = \dot{\varepsilon}_{1A} + \dot{\varepsilon}_{1B} = -\frac{2\dot{\varepsilon}_3 K}{R} \tag{2.24}$$

Based on Rowe's equation, D is defined as:

$$D = -\frac{2\dot{\varepsilon}_3}{\varepsilon_1'} \tag{2.25}$$

and the volumetric strain rate is defined as:

$$\dot{\varepsilon}_v = \dot{\varepsilon}_{1A} + \dot{\varepsilon}_{1B} = \frac{\dot{\varepsilon}_2}{D_A} + \frac{\dot{\varepsilon}_3}{D_B} \tag{2.26}$$

$$D_A = D_B = -\frac{1 - sin\psi}{1 + sin\psi} \tag{2.27}$$

Thus Schanz and Vermeer proposed the equation below in order to calculate dilatancy angle with respect to triaxial testing condition:

$$sin\psi = -\frac{\frac{\dot{\varepsilon}_v}{\dot{\varepsilon}_1}}{2 - \frac{\dot{\varepsilon}_v}{\dot{\varepsilon}_1}} \tag{2.28}$$

Schanz and Vermeer's work justified that plain-strain and triaxial tests provide almost same dilatancy angle. These two tests give the same result for the peak friction

angle as well. Schanz and Vermeer also concluded that the critical state friction angle should be taken into consideration as a distinctive parameter for cohesionless soil and is independent from relative density and confining pressure. They rearranged Bolton's Equation for dilatancy angle in terms of relative density index as below:

$$sin\psi = -\frac{0.3I_R}{2 + 0.3I_R} = \frac{I_R}{6.7 + I_R} \tag{2.29}$$

2.1.6. Vaid and Sasitharan Equation

Vaid and Sasitharan (1991), in their set of triaxial tests, examined how stress path affects dilatancy angle of sands. By the reason that in field, in practice, soil would be exposed to different loading conditions in comparison with the condition in triaxial compression they put stress path in their experiments. And they added α angle for loading condition. Within their consolidated drained triaxial tests, (α=0) when it was compression mode, (α=90) when extension mode. Erksak sand which passes through No.10 sieve and remains on No.100 sieve was used for testing. Sand samples were reconstituted in different relative densities with vibration method and consolidated under stresses varied between 100-2400 kPa. Shearing was applied in such manners that increasing and decreasing mean effective stresses.

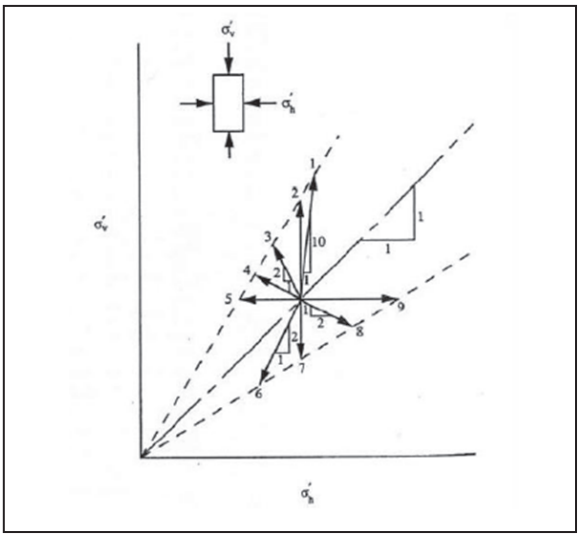


Figure 2.12. Stress Paths Applied in (Vaid and Sasitharan, 1991).

According to the results maximum dilatancy rate $\left(-\frac{d\varepsilon_v}{d\varepsilon_\alpha}\right)_{max}$ is observed when the stress-strain curve reaches the peak regardless of stress path or direction of loading. Another finding is that the compression tests give higher values of dilatancy rate than the extension tests. Also peak friction angle shows similar response as maximum dilatancy rate.

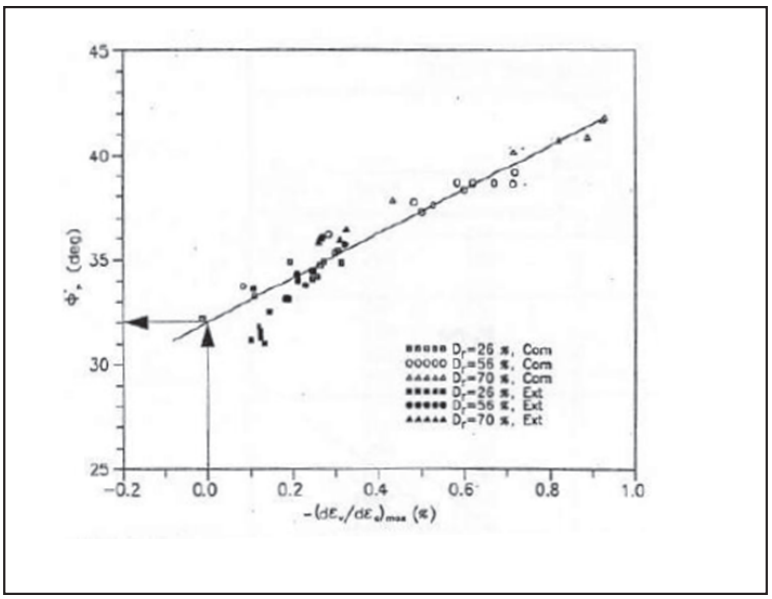


Figure 2.13. Relationship Between Peak Friction Angle and Maximum Dilatancy Rate (Vaid and Sasitharan, 1991).

Vaid and Sasitharan defined a relationship as below, according to the results shown in Figure 2.13:

$$\left|\frac{d\varepsilon_v}{d\varepsilon_a}\right|_{max} = 0.1\left(\phi'_{peak} - \phi'_{cv}\right) \tag{2.30}$$

and dilatancy angle in terms of triaxial testing as:

$$\psi = sin^{-1}\left[\frac{-d\varepsilon_v}{d\gamma}\right] = sin^{-1}\left[\frac{-d\varepsilon_v}{d\varepsilon_1 - d\varepsilon_3}\right] \tag{2.31}$$

In triaxial compression testing:

$$d\varepsilon_1 = d\varepsilon_a \tag{2.32}$$

$$d\varepsilon_3 = d\varepsilon_r = \frac{d\varepsilon_v - d\varepsilon_a}{2} \tag{2.33}$$

and the Equation 2.31 can be rearranged as:

$$\psi = sin^{-1}\left[\frac{2}{\frac{3}{d\varepsilon_v/d\varepsilon_a} + 1}\right] \tag{2.34}$$

In terms of triaxial extension testing:

$$d\varepsilon_3 = d\varepsilon_a \tag{2.35}$$

$$d\varepsilon_1 = d\varepsilon_r = \frac{d\varepsilon_v - d\varepsilon_a}{2} \tag{2.36}$$

Thus:

$$\psi = sin^{-1}\left[\frac{2}{\frac{3}{d\varepsilon_v/d\varepsilon_a} - 1}\right] \tag{2.37}$$

Vaid and Sasitharan revealed a linear relationship between dilatancy angle and peak friction angle within the plots drawn with the results of the equations they proposed. Hence they rearranged Bolton's equation regarding peak friction angle, critical state friction angle and dilatancy angle:

$$\phi'_{peak} = \phi'_{cv} + 0.33\psi \tag{2.38}$$

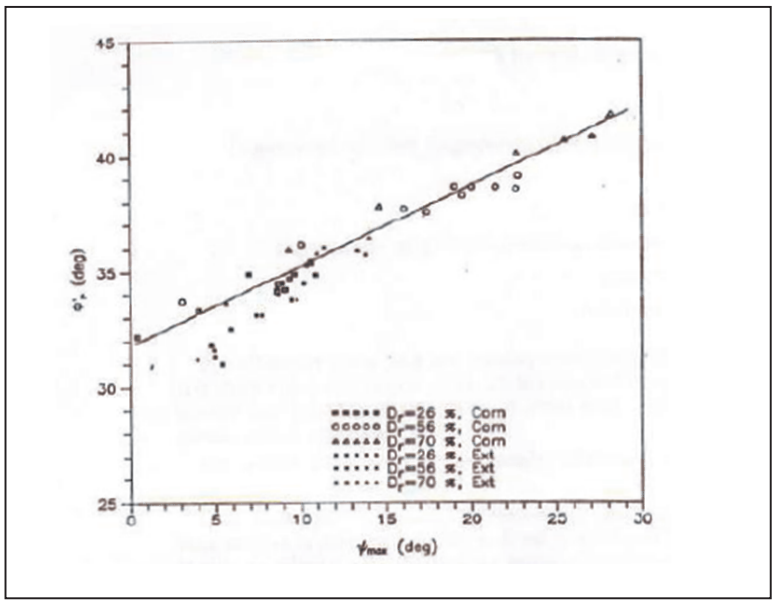


Figure 2.14. ϕ'_{peak}-ψ_{max} Plot in Terms of Both Triaxial Compression and Extension Tests (Vaid and Sasitharan, 1991).

2.1.7. Cinicioglu and Abadkon Equation

Cinicioglu and Abadkon (2014) established a link between dilatancy angle, pre-shear mean effective stress and relative density for cohesionless soils. They aimed to determine dilatancy angle at exploration phase of a design project. Within the scope of their work, an experimental study regarding triaxial tests on local Standard Ottawa sand was conducted. Beside their experiments, they examined the data of the study conducted by Vaid and Sasitharan (1992) on Erksak sand and proposed an equation to determine dilatancy angle by means of two unit independent soil constants:

$$tan\psi_p = \alpha_\psi \left(\frac{p'_i}{p_a}\right) + m_\psi I_D \tag{2.39}$$

where α_ψ and m_ψ are unit-independent fitting parameters which vary with relative density index I_D, ψ_p represents peak dilatancy angle, p'_i for pre-shear mean effective stress standard atmospheric pressure at sea level. α_ψ corresponds to the decrease in dilatancy angle per unit increase in normalized confinement whereas m_ψ corresponds to the increase in dilatancy angle per unit increase in relative density.

3. METHODOLOGY FOR THE TESTING OF ANALYZED SANDS

The objective of this study is to investigate strength parameters; peak dilatancy angle and peak friction angle, with the intention of selecting appropriate value as a design friction angle for different geotechnical engineering applications. As peak dilatancy angle for cohesionless soils can be obtained by in situ tests using mean effective stress and relative density, the decision of selecting whether peak or critical state friction angle as design friction angle can be feasible if a relationship between strength parameters and shear strain exists. For this purpose, the data of 70 triaxial compression tests conducted with Silivri sand were examined. Within those experiments, the reconstituted samples were consolidated under K_0 conditions and sheared drained. Overconsolidation ratio (OCR) and relative density (D_r) parameters varied in groups of experiments. In addition to this main source of data, triaxial compression test data of Erksak sand and Anatolian sands produced by Sasitharan (1989) and Erzin (2004), respectively, which is conducted under similar conditions, were used.

3.1. K_0 Triaxial Testing Program

Within the context of this study, 70 CD test data were examined under K_0 conditions. OCR, relative density and vertical effective stress at the end of consolidation stage (σ'_{vc}) were variables. All triaxial tests were conducted according to the ASTM (D7181) standard. An automatic triaxial testing apparatus manufactured by Geocomp was used which provides consolidation without lateral strain by automatically adjusting cell pressure to achieve K_0 conditions.

Table 3.1. Experimental Program.

Test No.	OCR	P'c (kPa)	Dr (%)
2	1	114.32	49%
3	1	226.38	100%
4	1	56.81	51%
5	1	32.19	49%
6	1	155.97	49%
7	1	112.29	64%
8	1	238.68	49%
9	1	284.33	49%
10	2	57.05	78%
11	2	114.55	82%
12	2	276.15	74%
13	2	464.75	87%
14	2	224.83	73%
15	2	299.47	60%
16	2	291.19	50%
17	2	657.98	91%
18	2	491.15	72%
19	2	64.9	47%
20	2	57.93	56%
21	2	233.74	54%
22	2	59.38	39%
23	2	30.46	55%
24	2	490.16	64%
25	2	251.29	53%
26	2	81.58	57%
27	2	119.04	50%
28	4	116.28	82%
29	4	579.05	80%
30	4	484.21	86%
31	4	1043.03	70%
32	4	582.95	86%
33	4	945.6	94%
34	4	522.89	63%
35	4	931.29	90%

Table 3.1. Experimental Program (Cont.).

Test No.	OCR	P'c (kPa)	Dr (%)
36	4	216.73	84%
37	4	468.22	72%
38	4	113.02	76%
39	4	238.38	57%
40	4	611.08	62%
41	4	118.03	82%
42	4	505.53	53%
43	4	638.61	55%
44	4	228.47	59%
45	4	119.29	52%
46	4	233.16	91%
47	4	499.58	61%
48	4	242.97	63%
49	4	61.94	41%
50	4	586.99	52%
51	4	120.36	41%
52	4	492.51	34%
53	4	245.79	34%
54	8	430.04	76%
55	8	932.98	87%
56	8	1073.78	63%
57	8	2050.71	97%
58	8	945.66	89%
59	8	1175.69	87%
60	8	1084.46	72%
61	8	111.3	55%
62	8	236.14	54%
63	8	229.56	57%
64	8	119.86	43%
65	8	463.75	57%
66	8	127.35	33%
67	8	235.81	55%
68	8	1289.99	68%
69	8	2128.57	79%
70	8	2083.02	76%

3.2. Testing Material

3.2.1. Silivri Sand

Silivri sand, which is classified as poorly graded sand (SP) with C_u value of 2.16 and C_c of 1.45, was used as the testing material in this study.

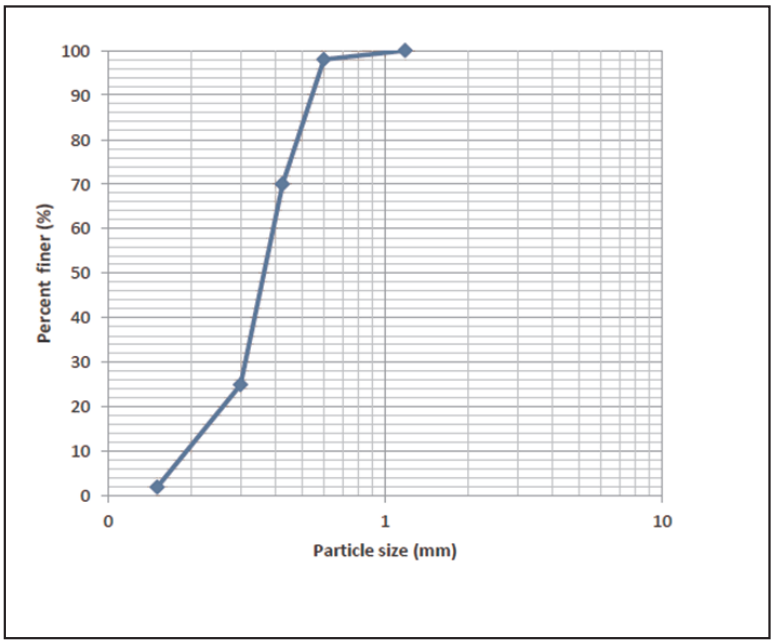


Figure 3.1. Grain Size Distribution of Silivri Sand.

Maximum and minimum void ratios of the testing material were obtained by relative density tests on vibratory table in accordance with the standards; ASTM D-4253 and ASTM D-4254. Due to test results, maximum and minimum void ratios of the sand were obtained as 0.96 and 0.56 respectively. An average value of 2.67 for specific gravity was determined as a result of a set of tests. The dry unit weight of the sand used in this study varied between 14.65 and 17.85 kN/m3.



Figure 3.2. Vibratory Table Used to Determine Maximum Minimum Void Ratios.

Following table shows main properties of the sand used in the triaxial tests:

Table 3.2. Main Properties of the Sand Used in this Study.

Sample	γ_{dry} (N/m^3)	G_s	e_{min}	e_{max}	D_{10}	D_{30}	D_{60}	D_{50}	C_c	C_u
Silivri Sand	14.65-17.85	2.67	0.56	0.96	0.184	0.325	0.397	0.365	1.45	2.16

3.2.2. Erksak Sand

The data obtained from the results of the experiments over Erksak sand conducted by Sasitharan (1989) was also used in this study. Throughout the work of Sasitharan (1989), samples of Erksak sand were prepared by first washing them to remove clay and silt particles. The sand was air dried and the fraction passing #10 sieve and retained on #100 sieve was used for testing. Also the sample ensured homogeneity among all test by following the sample preparation procedure mentioned above. Erksak sand is composed of subangular particles. The mineral composition is of 80% quartz, 10% feldspar, %10 other. The grain size distribution of the sand used in Sasithran's study is shown in Figure 3.3. The median grain size value, D_{50}, is 0.34 mm and specific gravity is 2.66. According to the method specified in ASTM D2049, the maximum and

minimum void ratios are 0.775 and 0.525 respectively. Also, coefficient of uniformity and coefficient of curvature are calculated as 1.90 and 1.00 by means of D10, D30 and D60.

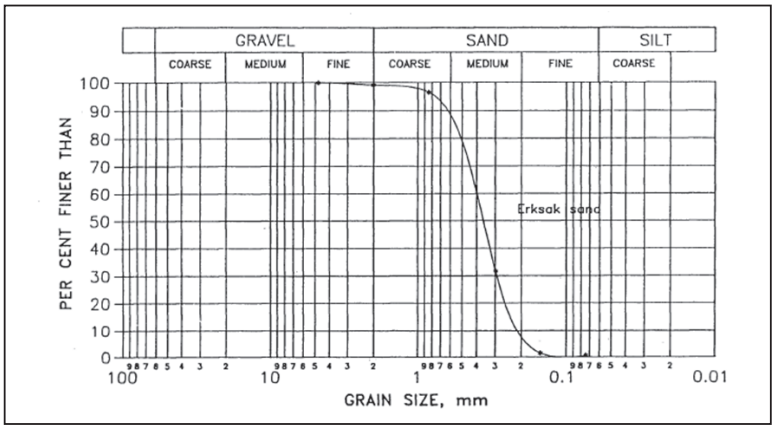


Figure 3.3. The Grain Size Distribution of Erksak Sand Used in Sasitharan's Study Adapted from (Sastitharan, 1989).

The properties of Erksak sand used are listed in the table below:

Table 3.3. Main Properties of the Sand Used in this Study.

Sample	G_s	e_{min}	e_{max}	D_{10}	D_{30}	D_{60}	D_{50}	C_c	C_u
Erksak Sand	2.66	0.525	0.775	0.21	0.29	0.4	0.34	1	1.9

3.2.3. Anatolian Sands

Another bulk of data produced by triaxial experiments of Erzin (2004) in which 6 different sands collected from different regions of Anatolia was used within this study. Sieve analyses were carried out in order to determine the initial gradation of the samples. Basic soil parameters determined from the gradation curve for each sample. Samples were named by letters from A to F.

Table 3.4. Locations of Samples Used in the Study of (Erzin, 2004).

Sample	Location
A	Sand quarry located 5 km south of Kazan, Ankara
B	Salt Lake sand located 6 km north-west of Şereflikoçhisar, Ankara
C	Sand quarry located 3 km west of Bafra, Samsun
D	Beach located 4 km west of Sinop
E	Sand hill located 8 km west of Yumurtalık, Adana
F	Sand quarry located 4 km west of Ceyhan, Adana

Based on the results of laboratory experiments over sands collected from different regions, main soil properties were summarized as shown in Table 3.5.

Table 3.5. Main Properties of Sands Used in (Erzin, 2004).

Sample	G_s	e_{max}	e_{min}	D_{10} (mm)	D_{30} (mm)	D_{60} (mm)	D_{50} (mm)	C_c	C_u
A	2.64	0.651	0.4	0.2	0.59	1.16	0.9	1.5	5.8
B	2.62	0.863	0.501	0.53	0.84	1.19	1.2	1.12	2.24
C	2.68	0.613	0.411	0.23	0.39	0.8	0.6	0.83	3.48
D	2.64	0.797	0.584	0.33	0.39	0.41	0.31	1.12	1.24
E	2.7	0.813	0.559	0.21	0.29	0.37	0.22	1.08	1.76
F	2.7	0.818	0.538	0.21	0.33	0.46	0.3	1.13	2.19

3.3. Sample Preparation

Air pluviation method chosen for preparation of sand samples in this study is a convenient way to reach target void ratios in such a way that dry sand is poured within a funnel to a mold from a predetermined height. Funnel is gradually moved upwards as the sand is poured in order to keep the raining height constant. By this means uniformity in sample is preserved as well.

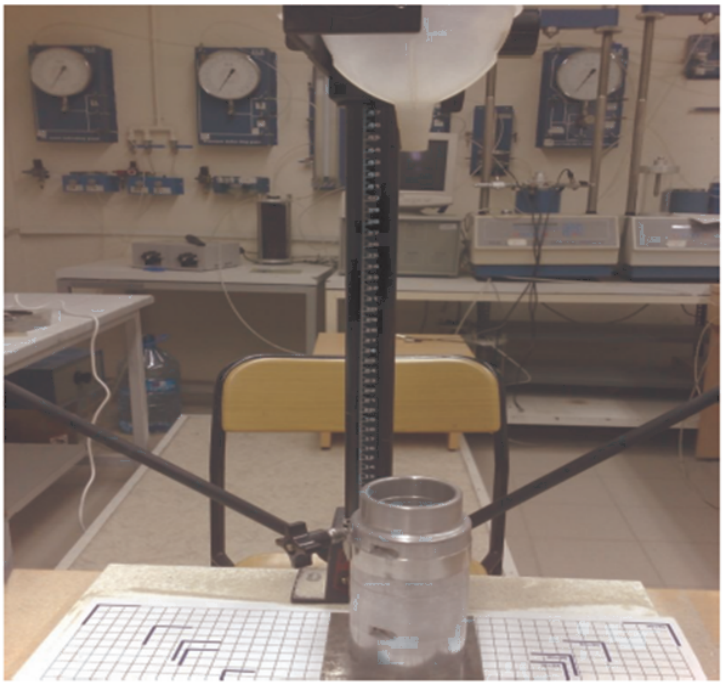


Figure 3.4. Air-Pluviation Set-Up.

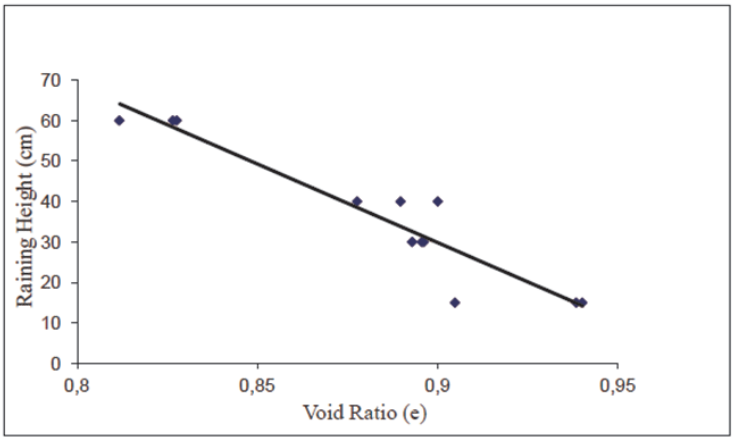


Figure 3.5. Variation of Void Ratios of Samples with Raining Height (Abadkon, 2012).

According to a set of air pluviaton tests, Kolbuzewsky (1948) declared that density of a sample which is prepared by air pluviation method is proportional to raining height. He proposed the equation below:

$$h = -388.53e + 379.5 \tag{3.1}$$

where h is the raining height in centimeter and e represents void ratio of the sample.

3.4. Automatic Triaxial Testing Apparatus

Automatic triaxial apparatus comprises of three main components as two automatic flow pumps (or tracs) and a computer controlled loading frame which contains a control system and the components to generate the force on the sample. Loading frame, also called the load trac, gauges the force and displacement during the test. Flow tracs are intelligent units created from a flow pump, a pressure sensor and a control board.

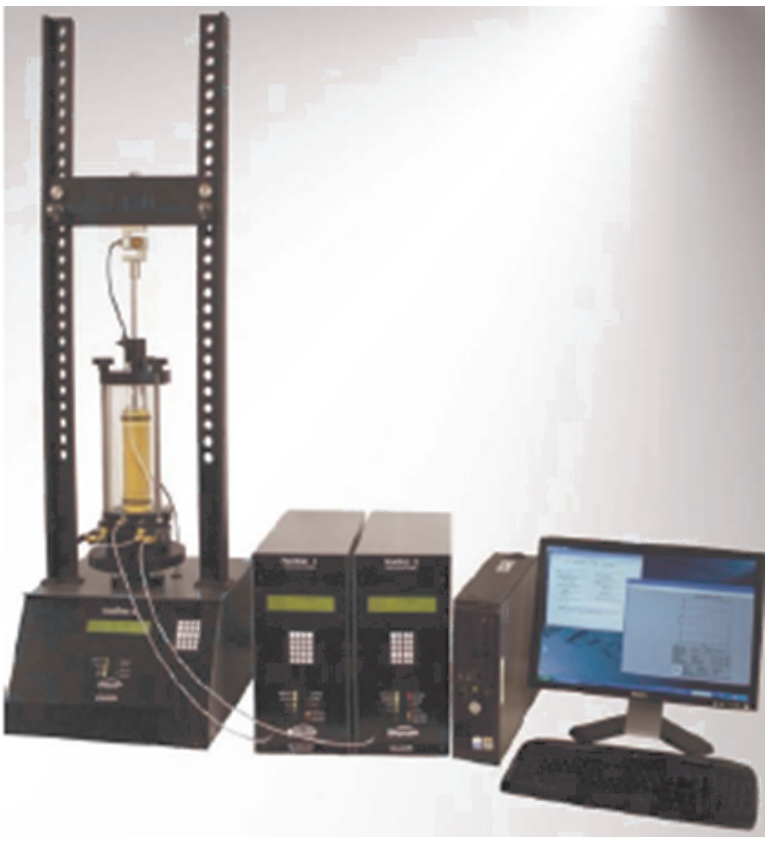


Figure 3.6. Automatic Triaxial Testing Apparatus.

Flow pumps in flow tracs set pressure and volume in test cell. Flow tracs contain precision micro stepper motor, which moves a piston in a water filled cylinder. Pressure transducers which mounted at the end of the cylinder, determine the signals being sent to the stepper motor and the number of motor steps is used to calculate the volume

changes. Flow tracs are capable of maintaining the required pressure within 0.35 kPa. Pressure increments can increase and decrease in any template by any amount. The count readings from sensors are converted to engineering units and calibration factors assure this transition.

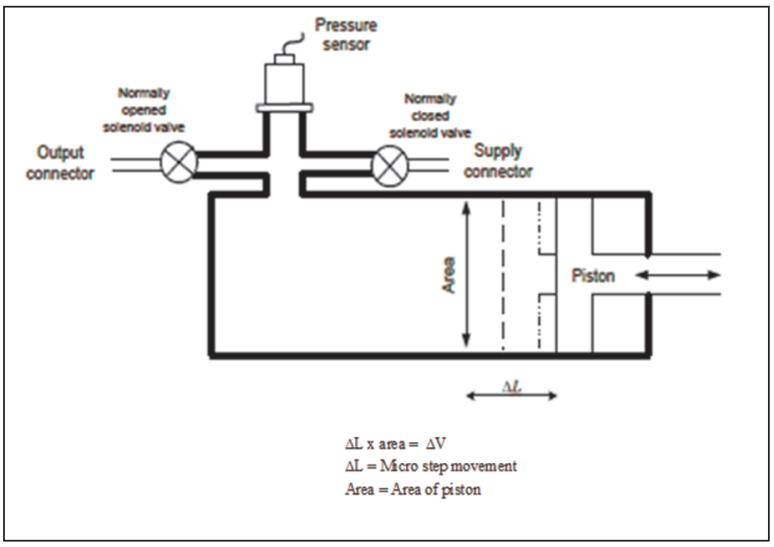


Figure 3.7. Schematic of a Flow Trac Unit.

3.5. Triaxial Testing Procedure

K_0 consolidated drained triaxial test was selected as the testing method in this research. Automatic triaxial apparatus guides consolidated drained triaxial tests in four stages as:

- Initialization
- Saturation
- Consolidation
- Shearing

3.5.1. Initialization Phase

A small horizontal and vertical stress along with the pore pressure is applied to the specimen during the initialization. It is done in order to make an observation that

the apparatus functions as required and there is no leakage of water from the valves of the apparatus and this phase takes about 20 minutes.

3.5.2. Saturation Phase

In saturation phase, cell and pore pressures are increased step-by-step while effective stress on the sample is kept stable in order to achieve the maximum saturation ratio. The increase in pore pressure is tracked by the system automatically when the increase in the cell pressure is applied. Pore pressure parameter is obtained from the below equation according to ASTM (D-7181):

$$B = \frac{\Delta u}{\Delta \sigma_3} \tag{3.2}$$

Where Δu is the change in the specimen pore pressure that occurs when cell pressure changes and specimen drainage valves are closed and $\Delta\sigma_3$ is the change in cell pressure. Before applying the next cell pressure increment, the pore pressure is raised and held stable in order to maintain the effective stress on the sample. A sample achieved a minimum Skempton value of B=0.95 is regarded as fully-saturated.

3.5.3. Consolidation Phase

Once reaching the Skempton value of 0.95, consolidation phase is started by the equipment automatically or manually. Lateral strains are restricted with respect to K_0 conditions. Cell pressure is adjusted by the automatic triaxial system with the aim of preventing the lateral straining during loading and unloading. Within the context of Abadkon's triaxial testing program, samples have been loaded and unloaded with a constant stress ratio of 5 kPa/min and to gain overconsolidation ratios of 1, 2, 4 and 8.

3.5.4. Shearing Phase

In shearing phase, vertical stress is increased with constant strain rate of 2.5x10-2%/min in order to shear samples. According to ASTM (D-7181), where $\dot{\varepsilon}$ shear strain rate and t_{90} is the time corresponding to 90% primary consolidation obtained from the following equation:

$$\dot{\varepsilon} = \frac{4\%}{10_{t90}} \tag{3.3}$$

Samples were sheared until they reached the maximum axial strain value of 20%. Critical state behavior of the sand was well observed by reaching this axial strain value.

3.6. Triaxial Test Corrections

In order to get realistic results from triaxial tests, there are some significant corrections to be done.

i) Piston area correction
ii) Rubber membrane correction
iii) Sample area correction

3.6.1. Piston Area Correction

Buoyancy force, which works for moving the piston upwards, affects the piston applying the vertical stress to the sample. For excluding the effect of buoyancy in vertical stress calculations, effective area of the piston is measured by filling the cell with water and applied pressure to the piston; then, buoyancy force is measured while the cell pressure is increasing. For the triaxial test program conducted by Abadkon (2012), results were plotted and the effective area of the piston was determined from the slope of the line relating the cell pressure and emerging buoyancy force as shown in Figure 3.8.

An effective are of 153 mm^2 was calculated for the experiments of Abadkon (2012). Therefore buoyancy force can be calculated from the following equation:

$$F_b = 0.153\sigma_c + 6.25 \tag{3.4}$$

where F_b represents the buoyancy force and σ_c stands for the cell pressure. The buoyancy force determined by this equation is subtracted from the total load value.

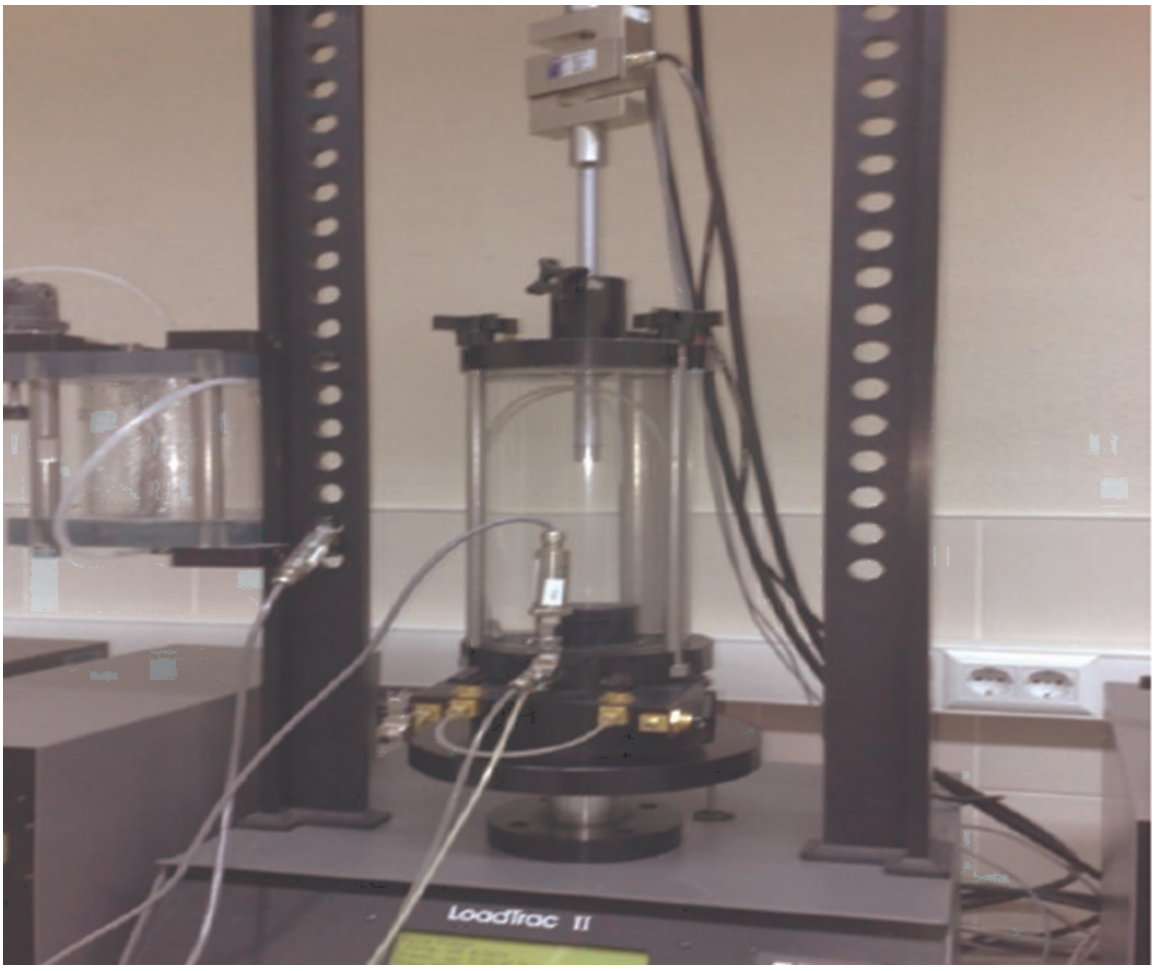


Figure 3.8. Piston Area Correction Test (Abadkon, 2012).

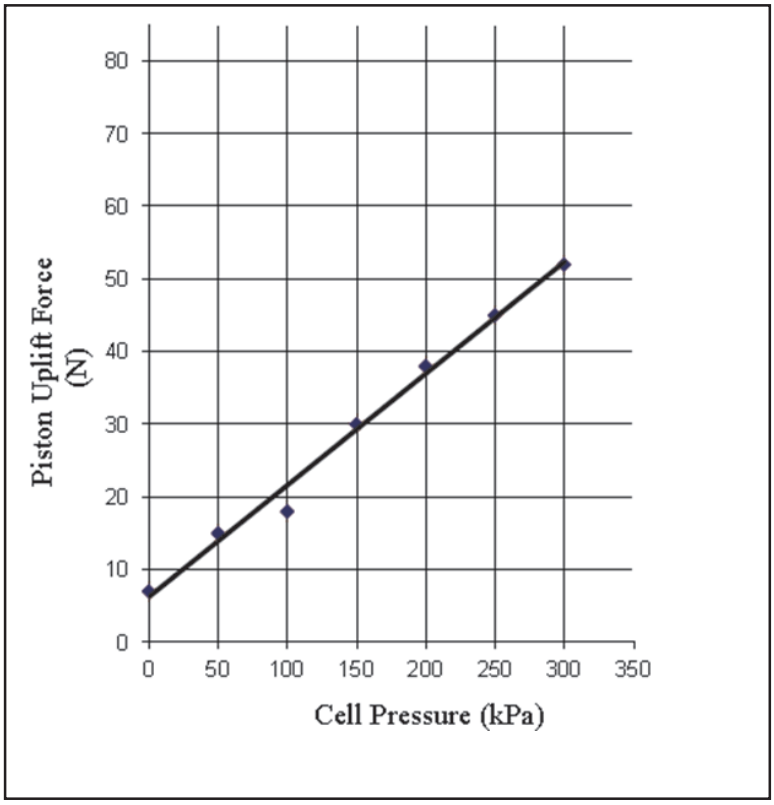


Figure 3.9. Variation of Uplift Force with Cell Pressure (Abadkon, 2012).

3.6.2. Correction for the Rubber Membrane

Thickness of the membrane is a parameter which affects the radial stress applying to the sample within triaxial tests. ASTM (D-4767) proposes the following equation in order to correct the principal stress difference for the effect of rubber membrane:

$$\Delta\left(\sigma_1 - \sigma_3\right) = \frac{4E_m t_m \varepsilon_1}{D_C} \tag{3.5}$$

where $\Delta(\sigma_1 - \sigma_3)$ stands for the correction to be subtracted from the deviator stress measured during the test, D_C is the diameter of the sample, E_m is the young's modulus for the membrane material, t_m is the membrane thickness and ε_1 is the axial strain. Young's modulus for the latex membrane is determined by a tensile test. The procedure of the test comprises pulling the membrane and measuring the observed strain. Young's modulus is determined by Equation 3.4. As a result of the tensile tests applied on the

membranes which are used for the study a value of 1450 kPa for the Young's modulus is obtained.

$$E_m = \frac{\left(\frac{F}{A_m}\right)}{\left(\frac{\Delta L}{L}\right)} \tag{3.6}$$

where E_m, F, L, ΔL,and A_m represent; the Young's modulus of the membrane material, the force applied to stretch the membrane, unstretched length of the membrane, the change in length of the membrane and the area of the membrane respectively. A_m can be obtained by the following equation:

$$A_m = 2t_m W_s \tag{3.7}$$

where t_m is the thickness of the membrane and W_s is the width of the circumferential strip.

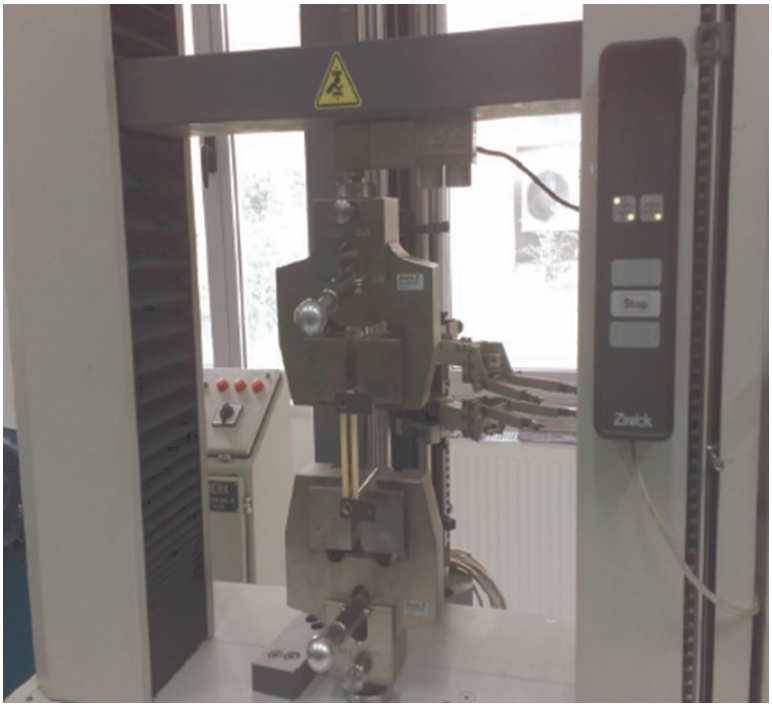


Figure 3.10. Tensile Test (Abadkon, 2012).

3.6.3. Correction for Sample Area

Depending on the change in the sample during the shearing phase, two kinds of area correction can be applied.

i) Uniform area correction (Figure 3.12)
ii) Parabolic area correction. (Figure 3.11)

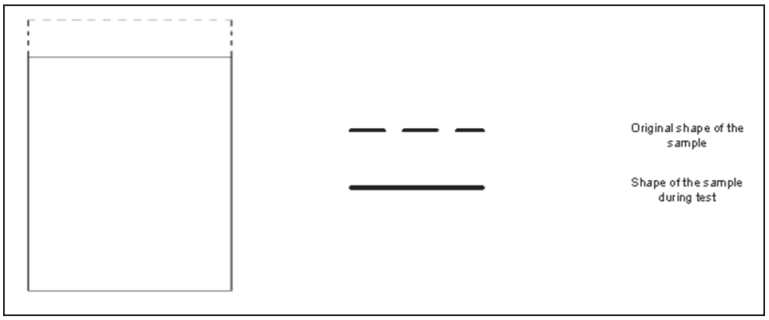


Figure 3.11. None Area Correction.

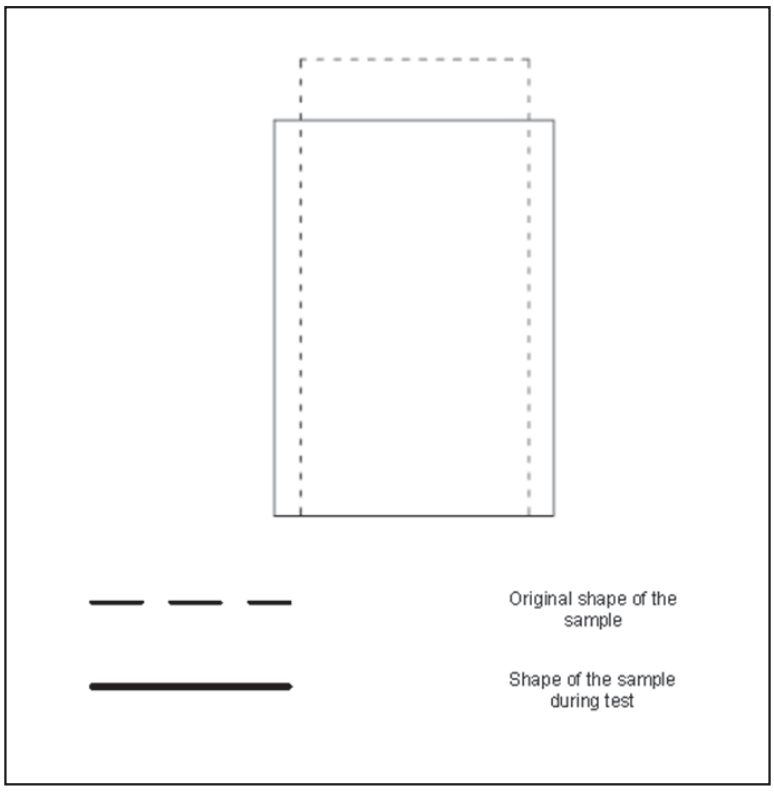


Figure 3.12. Uniform Area Correction.

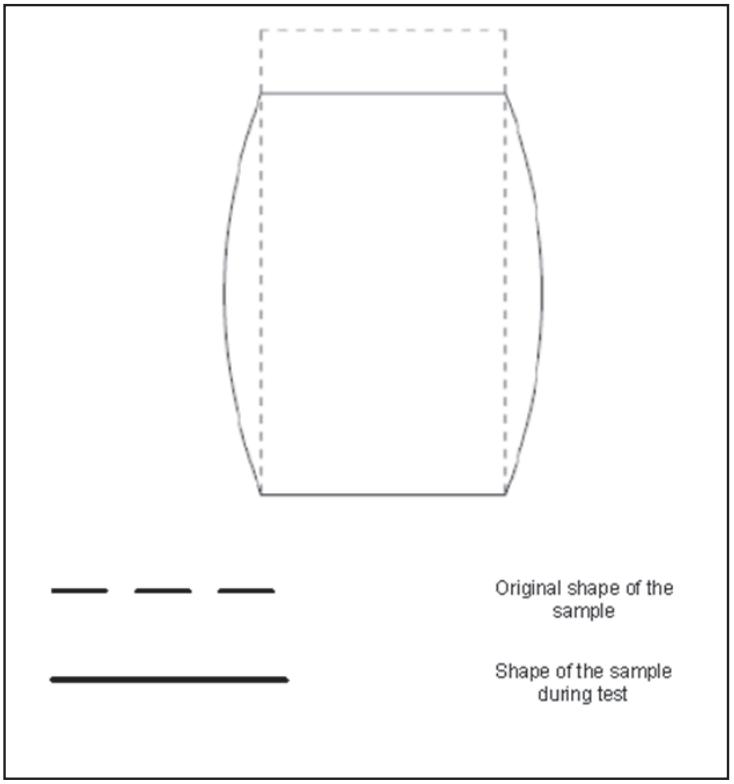


Figure 3.13. Parabolic Area Correction.

For samples having a parabolic shape during the shearing phase as shown in Figure 3.13, correction of the area change in vertical stress calculations has been done with the following equation:

$$A_c = A_0 \frac{1 - \varepsilon_v}{1 - \frac{5}{3}\varepsilon_1} \tag{3.8}$$

where A_c, A_0, ε_v, and ε_1 represent; the corrected area for the sample, the initial area of the sample, i the volumetric strain during shearing and the axial strain respectively. The following equation is used in order to obtain volumetric strain:

$$\varepsilon_v = \frac{\Delta V_s}{V_c} \tag{3.9}$$

where ΔV_s and V_c represent; the volume change of the sample during the shearing phase and the volume of the sample after the consolidation phase respectively. For axial strain, the equation below is used:



Figure 3.14. Parabolic Shape of the Sample During Shearing (Abadkon, 2012).

$$\varepsilon_1 = \frac{\Delta h}{h_c} \tag{3.10}$$

$$h_c = h_0 - \Delta h_0 \tag{3.11}$$

where h_0 represents the initial height of the sample and Δh_0 represents for the change of height in the specimen at the end of the consolidation phase.

4. EVALUATION OF TRIAXIAL TEST RESULTS

In this chapter, mainly the data obtained from triaxial compression tests conducted with Silivri sand are examined in terms of shear strain and dilatancy angle. Since the aim of this study is strain based selection of friction angle, mainly shear strain at failure - peak dilatancy angle response is investigated under different conditions.

In addition to the results of the experiments on Silivri sand, the data obtained from the studies of Sasitharan (1989) and Erzin (2004) are also used. Thus, 8 different sand samples acquired from 8 different lands were compared with each other with respect to their peak dilatancy angle-strain at failure response.

4.1. Results of the Triaxial Tests with Silivri Sand

Abadkon (2012), in his study, conducted 70 triaxial compression tests under drained K_0 conditions. Samples prepared with the help of air pluviation method were tested at various combinations of OCR (1, 2, 4 and 8). Confining pressures within tests were varied from 25 kPa to 1000 kPa. And also the samples were prepared at different relative densities (varying from 30% to 100%) for each different confining pressures and OCR combinations.

Table 4.1. Data Obtained From the Experiments Over Standard Ottawa Sand.

Test no.	OCR	P'$_f$ (kPa)	q$_f$ (kPa)	Ø'$_{peak}$ (deg)	Ø'$_{cs}$ (deg)	ε_{q-f} (%)	e$_{preshear}$	I$_D$(D$_R$)	I$_R$	ψ_p (deg)
1	1	85.06	129.71	37.45	29.53	4.048	0.7	0.64	2.58	10.7
2	1	152.49	241	38.71	33.41	4.563	0.76	0.49	1.95	5.89
3	1	294.42	466.46	38.81	32.62	5.107	0.55	1	3.3	12.01
4	1	66.63	97.56	36.06	29.71	3.821	0.75	0.51	2.46	8.26
5	1	43.71	59.98	33.96	27.73	6.556	0.76	0.49	2.57	8.68
6	1	212.39	309.97	35.93	33.22	8.298	0.76	0.49	1.79	4.46
7	1	145.59	232.57	39.09	33	4.467	0.7	0.64	2.57	8.89
8	1	319.74	485.48	37.29	32.72	7.284	0.76	0.49	1.58	1.59
9	1	334.91	482.67	35.53	33.44	10.410	0.76	0.49	1.57	0.1
10	2	72.17	120.92	40.89	30.34	3.778	0.64	0.78	3.47	14.07
11	2	132.58	225.12	41.45	30.4	4.569	0.62	0.82	3.21	13.77
12	2	257.2	425.11	40.38	33	5.203	0.66	0.74	2.3	9.28
13	2	456.44	742.43	39.78	33.75	7.175	0.6	0.87	2.37	8.01
14	2	220.19	356.17	39.56	33.57	6.818	0.66	0.73	2.35	9.84
15	2	321.41	470.72	36.06	33.06	8.110	0.72	0.6	1.53	5.34
16	2	348.92	534.39	37.59	34.38	7.284	0.75	0.5	1.09	3.28
17	2	452.95	740.4	39.96	35.34	6.716	0.59	0.91	2.52	6.51
18	2	457.71	677.23	36.4	33.64	8.942	0.67	0.72	1.78	4.46
19	2	97.86	145.38	36.54	30.95	6.629	0.77	0.47	1.53	7.65
20	2	57.93	81.58	34.79	29.12	5.741	0.73	0.56	2.34	9.91
21	2	295.57	457.19	37.94	34.14	6.509	0.74	0.54	1.34	5.31
22	2	67.69	94.45	34.49	31.47	7.764	0.8	0.39	1.28	6.47
23	2	37.18	48.77	32.59	26.5	2.971	0.74	0.55	2.48	10.08
24	2	437.58	630.3	35.5	35.71	12.186	0.7	0.64	1.51	2.98
25	2	262.32	376.9	35.42	32.97	9.569	0.74	0.53	1.37	5.25
26	2	84.63	127.94	37.13	31.68	4.691	0.73	0.57	2.15	9.44
27	2	138.6	216.14	38.22	31.89	6.740	0.76	0.5	1.51	7.27
28	4	98.11	162.46	40.43	33.95	5.062	0.61	0.85	3.61	15.15
29	4	353.16	572.78	39.67	31.27	5.436	0.63	0.8	2.31	9.39
30	4	453.39	715.96	38.69	34.48	6.193	0.61	0.86	2.32	9.88
31	4	656.95	954.95	35.81	30	12.316	0.67	0.7	1.45	1.64
32	4	371.19	597.34	39.38	40.75	7.246	0.61	0.86	2.51	10.31
33	4	521.84	813.19	38.21	32	6.477	0.57	0.94	2.52	8.37
34	4	330.99	478.49	35.62	33.8	12.449	0.7	0.63	1.66	6.47
35	4	508.58	839.08	40.32	33.86	5.565	0.59	0.9	2.38	8.14
36	4	175.21	304.49	42.36	31.89	5.344	0.62	0.84	3.05	13.69
37	4	385.31	592.19	37.72	34.01	8.690	0.66	0.72	1.93	7.87
38	4	86.41	138.35	39.18	31.45	4.659	0.65	0.76	3.22	13.52
39	4	176.78	300.86	41.52	32.83	4.987	0.73	0.57	1.76	8.46
40	4	356.69	526.98	36.36	35.22	9.839	0.71	0.62	1.54	5.39

Table 4.2. Data Obtained From the Experiments Over Standard Ottawa Sand (Cont.).

Test no.	OCR	P'$_f$ (kPa)	q$_f$ (kPa)	Ø'$_{peak}$ (deg)	Ø'$_{cs}$ (deg)	ε_{q-f} (%)	e$_{preshear}$	I$_D$(D$_R$)	I$_R$	ψ_p (deg)
41	4	91.96	143.24	38.2	30.41	4.704	0.63	0.82	3.48	14.5
42	4	356.68	531.16	36.63	34.38	9.498	0.74	0.53	1.19	4.27
43	4	448.16	649.84	35.72	33.55	9.483	0.74	0.55	1.13	2.83
44	4	150.85	238.24	38.7	33.09	5.401	0.72	0.59	1.93	8.93
45	4	103.4	150.62	35.87	32.26	5.158	0.75	0.52	1.8	8.65
46	4	187.24	324.26	42.2	35.98	2.859	0.59	0.91	3.33	14.92
47	4	299.03	446.6	36.72	36.37	9.694	0.71	0.61	1.64	6.47
48	4	166.84	257.57	37.87	33.03	5.183	0.7	0.63	2.07	9.49
49	4	44.33	55.08	30.96	27.06	4.066	0.79	0.41	1.55	7.3
50	4	316.27	478.95	37.2	36.5	8.110	0.74	0.52	1.23	4.03
51	4	93.25	129.42	34.3	32.56	7.511	0.79	0.41	1.26	6.55
52	4	320.14	471.2	36.22	35.78	12.130	0.82	0.34	0.46	0.9
53	4	143.99	201.65	34.58	33.57	8.242	0.82	0.34	0.73	4
54	8	115.41	195.94	41.39	32.98	2.862	0.65	0.76	3.01	12.81
55	8	337.27	579.01	41.86	35.27	4.246	0.6	0.87	2.63	11.68
56	8	394.49	585.63	36.51	33.8	10.896	0.7	0.63	1.54	5.79
57	8	613.03	1013.08	40.38	35.76	7.188	0.56	0.97	2.48	8.41
58	8	376.77	616.59	40.01	35.06	4.968	0.59	0.89	2.64	11.58
59	8	419.81	700.31	40.74	32.78	2.328	0.6	0.87	2.43	10.13
60	8	431.13	652.2	37.17	32.81	7.510	0.66	0.72	1.84	7.24
61	8	71.64	110.08	37.67	30.42	3.120	0.73	0.55	2.15	9.88
62	8	132.48	201.66	37.36	33.06	6.165	0.74	0.54	1.75	8.69
63	8	87.32	129.32	36.44	31.32	4.730	0.73	0.57	2.13	9.65
64	8	58.25	78.76	33.49	26.93	5.017	0.78	0.43	1.54	7.58
65	8	198.19	318.38	39.3	33.19	4.443	0.73	0.57	1.7	8.19
66	8	68.3	92.88	33.69	32.09	7.216	0.82	0.33	0.9	5.47
67	8	95.76	142.03	36.5	34.39	7.124	0.74	0.55	1.98	9.18
68	8	492.78	725.99	36.26	33.16	9.678	0.68	0.68	1.57	4.98
69	8	607.48	923.2	37.32	34.56	9.268	0.63	0.79	1.85	4.44
70	8	717.97	1101.43	37.65	34.45	6.660	0.65	0.76	1.59	2.62

Results based on the data of Abadkon's (2012) experiments are summarized in Table 4.1. Shear strain at failure, ε_{q-f}, was obtained from the equation shown below by means of axial strain, ε_a, and radial strain, ε_r, at failure which were also calculated from step motor outputs of the triaxial test device:

$$\varepsilon_q = \frac{2\left(\varepsilon_a - \varepsilon_r\right)}{3} \tag{4.1}$$

The peak dilatancy angle shown in Table 4.1 was obtained by the equation which was proposed by Schanz and Vermeer (1996) as below: which was explained in Section 3.

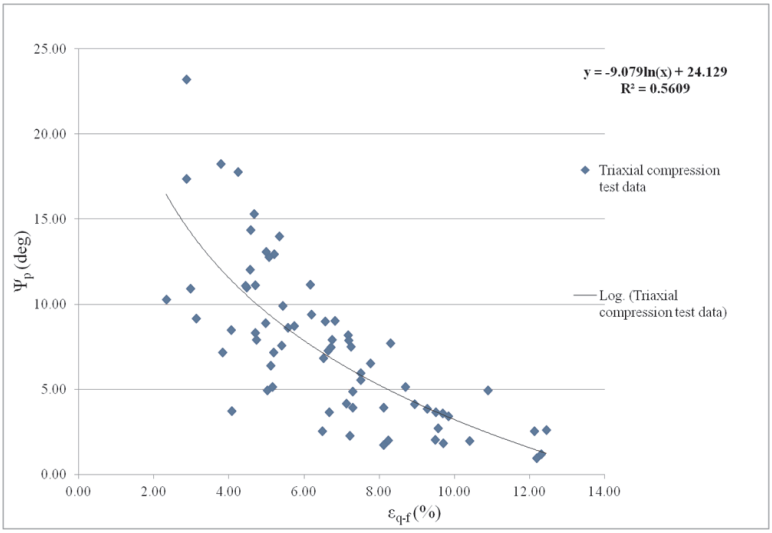


Figure 4.1. Peak Dilatancy Angle-Shear Strain at Failure Response Based on the Triaxial Experiments Over Silivri Sand.

According to the results of 70 different triaxial compression tests on Silivri sand as summarized in Table 4.1, the relationship between peak dilatancy angles and shear strain at failure, or in other saying, the shear strain occurring at the point where the peak dilatancy angle observed is shown in Figure 4.1. A natural logarithmic trendline is drawn as:

$$y = -9.079ln(x) + 24.129 \tag{4.2}$$

The equation can be rearranged as:

$$\psi_p = -9.079 \ln(\varepsilon_q) + 24.129 \tag{4.3}$$

$$\varepsilon_q = e^{\frac{\psi_p - 24.129}{-9.079}} \tag{4.4}$$

where ε_q represents shear strain and ψ_p is peak dilatancy angle.

4.2. Results of the Triaxial Tests with Erksak Sand

In the study of Sasitharan (1989), it was attempted to study the effect of consolidation history and stress path on stress strain and the failure strength by conducting drained triaxial tests. The effect of consolidation history was studied by consolidating samples of given relative density under anisotropic and hydrostatic conditions and shearing them in compression at constant confining pressure. In order to investigate the effect of stress path, samples were consolidated hydrostatically and then sheared under a variety of stress paths, both in compression and extension. Due to the material, Erksak sand, used within his experiments and the similarity in test techniques with the ones of Abadkon (2012), the data obtained from Sasitharan's (1989) conventional triaxial tests over Erksak sand was evaluated with respect to peak dilatancy angle and shear strain at failure. Results were summarized as shown in Table 4.2.

Table 4.3. Summary of the Data Obtained From Sasitharan's (1989) Study.

			At peak strength						
Test no.	Loading mode	D_r (%)	σ_3 (kPa)	ε_a (%)	ε_v (%)	ε_r (%)	ε_q (%)	$d\varepsilon_v/d\varepsilon_a$	ψ_p (degree)
C	Compression	0.56	250	3.402	-1.262	-2.332	3.823	-0.522	11.95
E	Extension	0.56	250	3.581	-0.03	-1.805	3.591	-0.18	4.74
1	Compression	0.26	250	6.722	-1.200	-3.961	7.122	-0.253	6.44
2	Compression	0.26	250	6.303	-1.278	-3.791	6.730	-0.306	7.63
3	Compression	0.26	250	3.272	-0.733	-2.003	3.516	-0.266	6.75
4	Compression	0.26	250	3.843	-0.96	-2.402	4.163	-0.291	7.3
5	Compression	0.26	250	3.710	-1.222	-2.466	4.117	-0.394	9.47
N/A	Compression	0.26	250	6.487	-1.114	-3.800	6.858	-0.184	4.82
N/A	Compression	0.7	250	2.595	-1.346	-1.970	3.043	-0.73	15.5
N/A	Compression	0.2	2400	13.269	1.660	-5.804	12.716	0.005	-0.14
N/A	Compression	0.56	2400	8.790	0.128	-4.331	8.748	-0.075	2.08
6	Extension	0.26	250	-4.089	-0.132	1.978	-4.045	-0.09	2.47
7	Extension	0.26	250	-5.870	-0.012	2.929	-5.866	0.092	-2.77
8	Extension	0.26	250	-5.806	0.113	2.959	-5.843	0.134	-4.13

According to the results of the conventional compression tests listed in Table 4.2, variation of peak dilatancy angle with shear strain at failure is illustrated in Figure 3.3. Similar responses with the results of Abadkon's (2012) experiments on Silivri sand

was observed in Erksak sand results. The trendline function fit to the plot is as below:

$$y = -8.491ln\,(x) + 21.667 \tag{4.5}$$

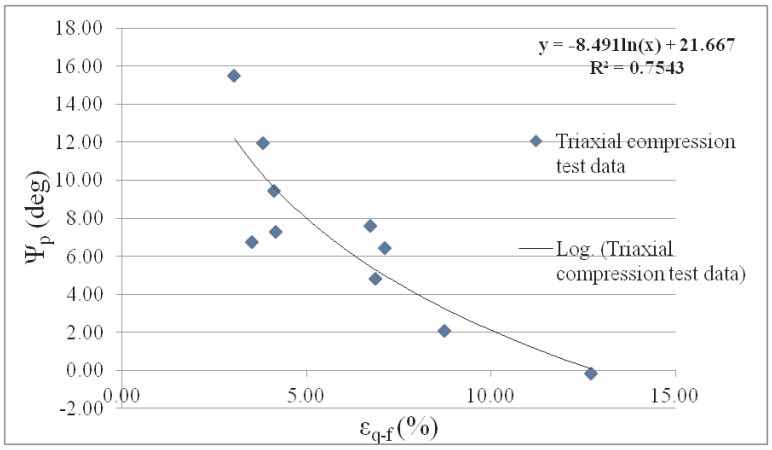


Figure 4.2. Variation of Peak Dilatancy Angle With Shear Strain at Failure for Erksak Sand.

The function defining the relationship between shear strain and peak dilatancy angle for Erksak sand can be rearranged as:

$$\psi_p = -8.491\ln(\varepsilon_q) + 21.667 \tag{4.6}$$

$$\varepsilon_q = e^{\frac{\psi_p - 21.667}{-8.491}} \tag{4.7}$$

4.3. Results of the Triaxial Tests with Anatolia Sands

In the study of Erzin (2004), Anatolian sands were obtained from different locations in Turkey in order to investigate the difference in strength measured in the wedge shear test, which approaches the plane strain condition, in the triaxial test, and in the shear box test. These locations were in Şereflikoçhisar (Ankara), Bafra (Samsun), Sinop, Ceyhan (Adana), and Yumurtalık (Adana) as listed in Table 3.4. In addition to

these, one more sample was obtained from Kazan (Ankara). The triaxial compression test data provided by this study constitutes a significant part of the comparison of different type of sands with respect to their peak dilatancy angle-shear strain at failure response.

6 different tables shown below summarize the results of Erzin's triaxial compression test program which are conducted under drained conditions. In these tables made up with excel spreadsheets; "At peak strength" indicates that the values below represent the ones at failure of samples as a result of shearing. All the parameters specified on tables are calculated in the same manner with those of Erksak and Silivri sand.

Table 4.4. Results of Experiments Conducted with Specimens of A.

			At peak strength						
Test no.	e	D_r (%)	σ_3 (kPa)	ε_a (%)	ε_v (%)	ε_r (%)	ε_q (%)	$d\varepsilon_v/d\varepsilon_a$	ψ_p (degree)
1	0.488	66.8	24.8	2.6	-1.4	-2	3.07	-0.93	18.51
2	0.487	67.2	38	3.8	-2.4	-3.1	4.6	-0.71	15.19
3	0.482	69.1	58.6	3.6	-1.6	-2.6	4.13	-0.71	15.19
4	0.476	71.3	79.6	3.8	-1.3	-2.55	4.23	-0.63	13.86
5	0.474	72.1	101.7	3.3	-0.7	-2	3.53	-0.54	12.27
6	0.479	70.2	136.8	3.6	-0.8	-2.2	3.87	-0.61	13.52
7	0.481	69.4	175.7	4.9	-0.7	-2.8	5.13	-0.38	9.19

Table 4.5. Results of Experiments Conducted with Specimens of B.

			At peak strength						
Test no.	e	D_r (%)	σ_3 (kPa)	ε_a (%)	ε_v (%)	ε_r (%)	ε_q (%)	$d\varepsilon_v/d\varepsilon_a$	ψ_p (degree)
1	0.628	64.4	14.2	2	-1.2	-1.6	2.4	-1	19.47
2	0.635	62.5	36.9	3.5	-1.1	-2.3	3.87	-0.74	15.67
3	0.63	63.9	47.9	2.3	-1	-1.65	2.63	-0.79	16.45
4	0.624	65.5	77.5	3.4	-0.7	-2.05	3.63	-0.47	10.97
5	0.616	67.8	108.5	3.8	-0.6	-2.2	4	-0.44	10.39
6	0.623	65.8	134	5.2	-0.4	-2.8	5.33	-0.28	7.05

Table 4.6. Results of Experiments Conducted with Specimens of C.

			At peak strength						
Test no.	e	D_r (%)	σ_3 (kPa)	ε_a (%)	ε_v (%)	ε_r (%)	ε_q (%)	$d\varepsilon_v/d\varepsilon_a$	ψ_p (degree)
1	0.552	31.6	11.3	1.5	-0.7	-1.1	1.73	-0.94	18.65
2	0.554	30.6	36.2	2.2	-0.8	-1.5	2.47	-0.67	14.53
3	0.565	69.1	47.9	2.7	-0.8	-1.75	2.97	-0.58	12.99
4	0.564	25.7	58.5	2.7	-0.7	-1.7	2.93	-0.55	12.46
5	0.579	18.4	75.4	3.7	-0.7	-2.2	3.93	-0.45	10.58
6	0.57	22.8	96	3.7	-0.8	-2.25	3.97	-0.46	10.78
7	0.556	29.6	153.9	4.5	-0.4	-2.45	4.63	-0.31	7.71

Table 4.7. Results of Experiments Conducted with Specimens of D.

			At peak strength						
Test no.	e	D_r (%)	σ_3 (kPa)	ε_a (%)	ε_v (%)	ε_r (%)	ε_q (%)	$d\varepsilon_v/d\varepsilon_a$	ψ_p (degree)
1	0.648	70	17.7	3.1	-2	-2.55	3.77	-0.85	17.35
2	0.643	72.3	23.1	2.7	-1.6	-2.15	3.23	-0.85	17.35
3	0.649	69.5	33.5	5.1	-2.3	-3.7	5.87	-0.53	12.09
4	0.649	69.5	55.5	2.7	-1.1	-1.9	3.07	-0.66	14.37
5	0.645	71.4	98.9	3.2	-1.1	-2.15	3.57	-0.65	14.2
6	0.645	71.4	120.7	5.3	-1.7	-3.5	5.87	-0.51	11.72
7	0.615	85.4	16.2	1.4	-1	-1.2	1.73	-1.12	21.04
8	0.618	84	24.5	2.5	-1.6	-2.05	3.03	-0.84	17.2
9	0.616	85	48.6	2.4	-0.9	-1.65	2.7	-0.9	18.08
10	0.617	84.5	95.5	2.7	-1	-1.85	3.03	-0.83	17.05
11	0.615	85.4	125.8	4.7	-1.2	-2.95	5.1	-0.66	14.37
12	0.618	84	153.4	2.7	-1.1	-1.9	3.07	-0.76	15.98

Table 4.8. Results of Experiments Conducted with Specimens of E.

			At peak strength						
Test no.	e	D_r (%)	σ_3 (kPa)	ε_a (%)	ε_v (%)	ε_r (%)	ε_q (%)	$d\varepsilon_v/d\varepsilon_a$	ψ_p (degree)
1	0.654	64	17.6	1.9	-0.8	-1.35	2.17	-1	19.47
2	0.654	64	24.5	1.4	-0.8	-1.1	1.67	-0.46	10.78
3	0.651	65.2	41.7	2.4	-0.9	-1.65	2.7	-0.97	19.06
4	0.654	64	76.2	2.2	-0.7	-1.45	2.43	-0.81	16.75
5	0.651	65.2	114	3.7	-0.7	-2.2	3.93	-0.48	11.16
6	0.653	64.4	148.5	4.8	-0.5	-2.65	4.97	-0.35	8.57
7	0.616	78.4	21.7	1.4	-1.2	-1.3	1.8	-1.65	26.88
8	0.616	78.4	36.8	1.8	-1	-1.4	2.13	-1.53	25.69
9	0.611	80.3	51.3	2	-0.8	-1.4	2.27	-1.3	23.2
10	0.615	78.8	103.6	3	-0.6	-1.8	3.2	-0.83	17.05
11	0.615	78.8	142.3	2.2	-0.8	-1.5	2.47	-0.76	15.98
12	0.615	78.8	167.2	2.7	-0.6	-1.65	2.9	-0.65	14.2

Table 4.9. Results of Experiments Conducted with Specimens of F.

			At peak strength						
Test no.	e	D_r (%)	σ_3 (kPa)	ε_a (%)	ε_v (%)	ε_r (%)	ε_q (%)	$d\varepsilon_v/d\varepsilon_a$	ψ_p (degree)
1	0.636	64.6	16.2	1.4	-0.7	-1.05	1.63	-1.08	20.53
2	0.634	65.3	25.1	1.6	-0.6	-1.1	1.8	-1.03	19.87
3	0.635	65	38.2	2.6	-1.1	-1.85	2.97	-0.68	14.7
4	0.634	65.3	70.7	3.3	-1	-2.15	3.63	-0.7	15.03
5	0.635	65	120.9	4	-0.8	-2.4	4.27	-0.5	11.54
6	0.632	66.1	151.3	5.2	-0.9	-3.05	5.5	-0.42	9.99
7	0.579	85.2	21	1.1	-0.3	-0.7	1.2	-1.4	24.32
8	0.58	84.8	31.3	2	-1	-1.5	2.33	-1.26	22.74
9	0.58	84.8	48.6	2.2	-0.9	-1.55	2.5	-1.17	21.66
10	0.58	84.8	97.6	3.7	-0.9	-2.3	4	-0.74	15.67
11	0.582	84.1	126.5	3	-0.8	-1.9	3.27	-0.66	14.37
12	0.579	85.2	165.2	3.9	-1.1	-2.5	4.27	-0.47	10.97

According to the results obtained as listed in Table 4.3, Table 4.4, Table 4.5, Table 4.6, Table 4.7, and Table 4.8, variations of peak dilatancy angle with shear strain at failure were drawn as figures below:

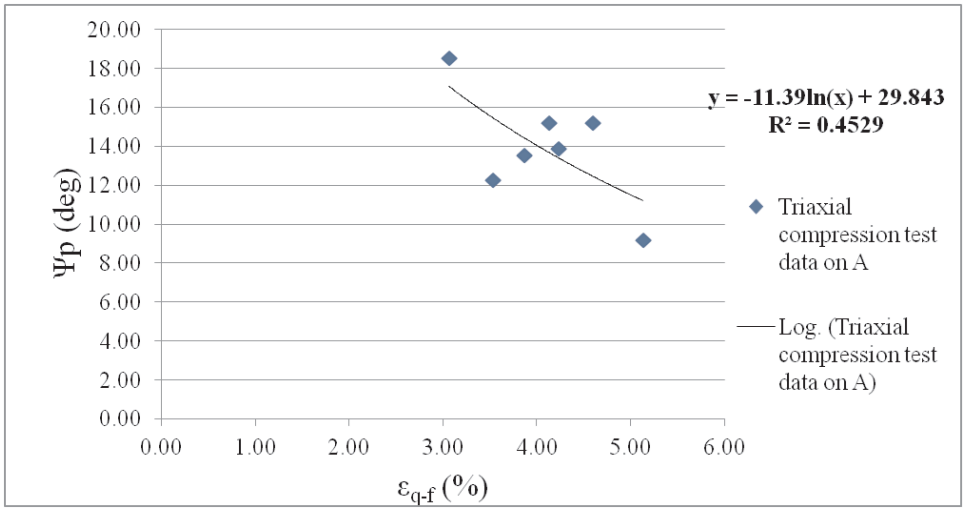


Figure 4.3. Peak Dilatancy Angle-Shear Strain at Failure Response of Specimen A.

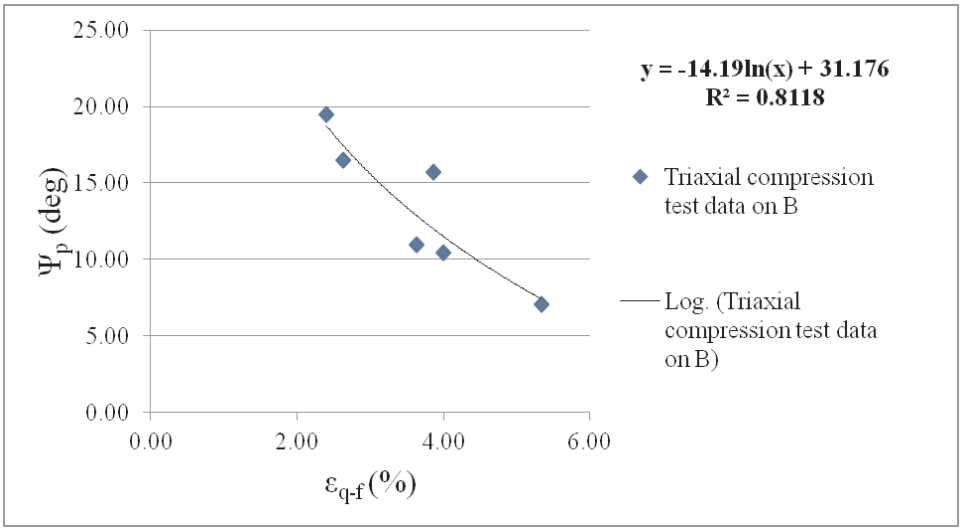


Figure 4.4. Peak Dilatancy Angle-Shear Strain at Failure Response of Specimen B.

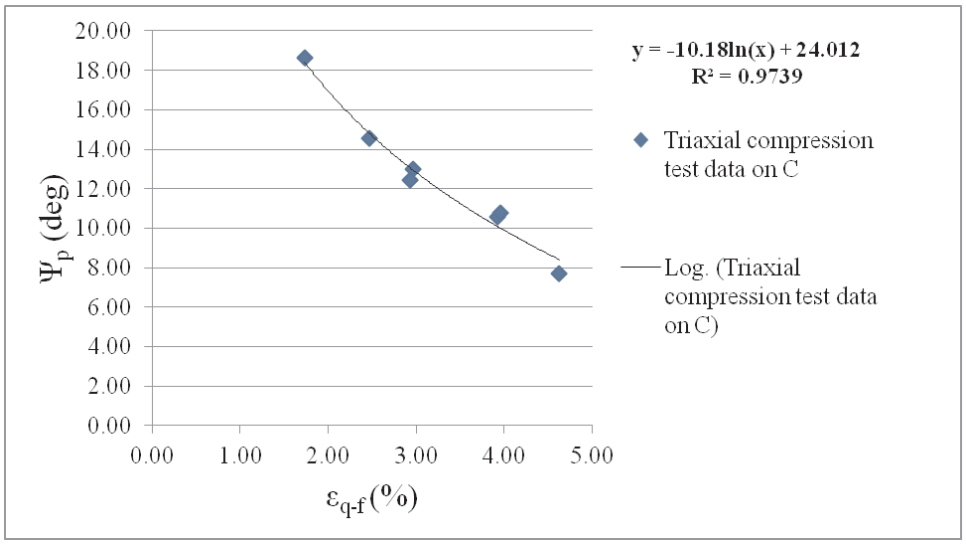


Figure 4.5. Peak Dilatancy Angle-Shear Strain at Failure Response of Specimen C.

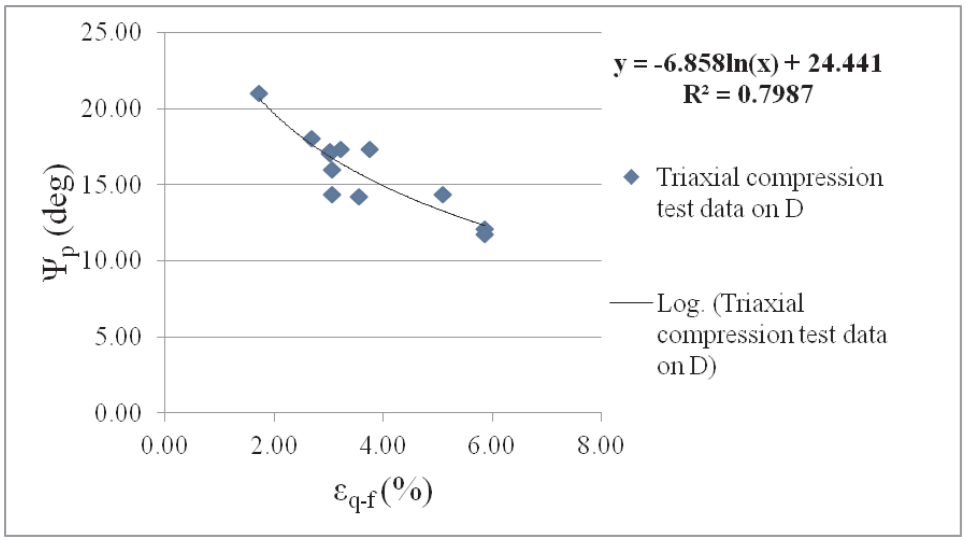


Figure 4.6. Peak Dilatancy Angle-Shear Strain at Failure Response of Specimen D.

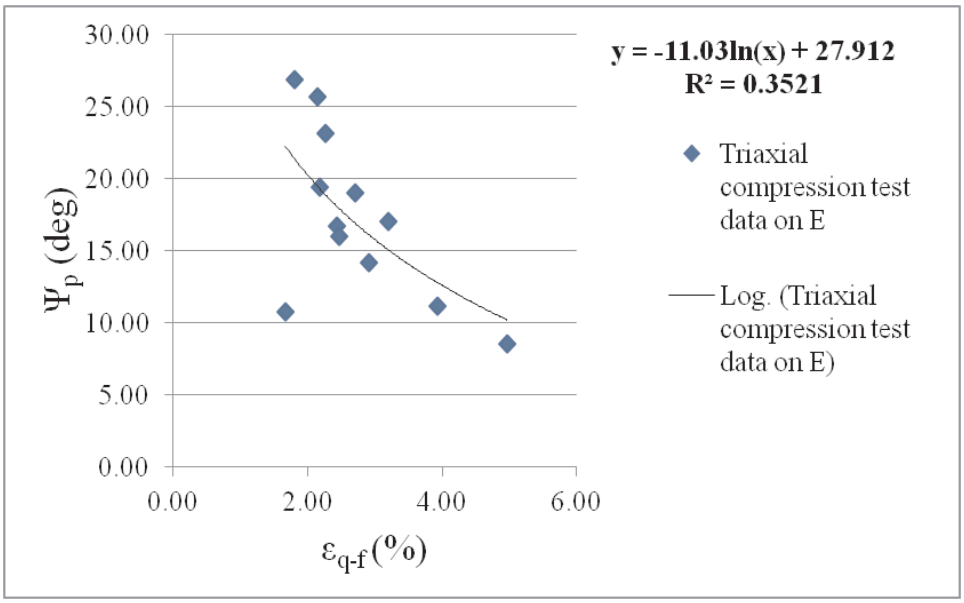


Figure 4.7. Peak Dilatancy Angle-Shear Strain at Failure Response of Specimen E.

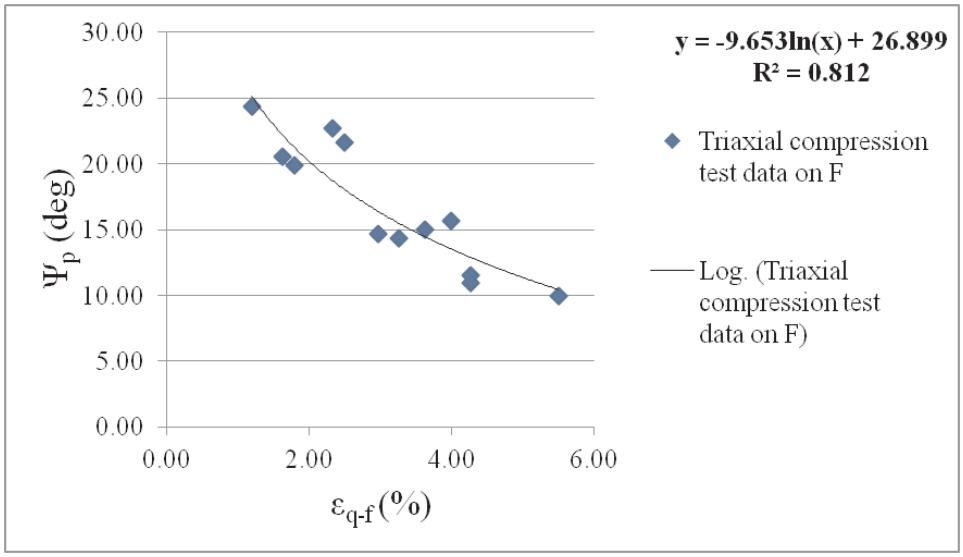


Figure 4.8. Peak Dilatancy Angle-Shear Strain at Failure Response of Specimen F.

As observed in figures above, results of the set of experiments conducted with 6 different sands throughout the study of Erzin (2004) showed considerable similarity with those of Abadkon (2012) and Sasitharan (1989) in terms of relationship between peak dilatancy angle and shear strain. The natural logarithmic trends and the empirical equations for each of the Anatolian sands are as below: For specimen A:

$$y = -11.39ln\,(x) + 29.843 \tag{4.8}$$

$$\psi_p = -11.39\ln(\varepsilon_q) + 29.843 \tag{4.9}$$

$$\varepsilon_q = e^{\frac{\psi_p - 29.843}{-11.39}} \tag{4.10}$$

For specimen B:

$$y = -14.19ln\,(x) + 31.176 \tag{4.11}$$

$$\psi_p = -14.19 \ln(\varepsilon_q) + 31.176 \tag{4.12}$$

$$\varepsilon_q = e^{\frac{\psi_p - 31.176}{-14.19}} \tag{4.13}$$

For specimen C:

$$y = -10.18 ln(x) + 24.012 \tag{4.14}$$

$$\psi_p = -10.18 \ln(\varepsilon_q) + 24.012 \tag{4.15}$$

$$\varepsilon_q = e^{\frac{\psi_p - 24.012}{-10.18}} \tag{4.16}$$

For specimen D:

$$y = -6.858 ln(x) + 24.441 \tag{4.17}$$

$$\psi_p = -6.858 \ln(\varepsilon_q) + 24.441 \tag{4.18}$$

$$\varepsilon_q = e^{\frac{\psi_p - 24.441}{-6.858}} \tag{4.19}$$

For specimen E:

$$y = -11.03 ln(x) + 27.912 \tag{4.20}$$

$$\psi_p = -11.03 \ln(\varepsilon_q) + 27.912 \tag{4.21}$$

$$\varepsilon_q = e^{\frac{\psi_p - 27.912}{-11.03}} \tag{4.22}$$

For specimen F:

$$y = -9.653ln\,(x) + 26.899 \tag{4.23}$$

$$\psi_p = -9.653\ln(\varepsilon_q) + 26.899 \tag{4.24}$$

$$\varepsilon_q = e^{\frac{\psi_p - 26.899}{-9.653}} \tag{4.25}$$

5. DISCUSSION

In this chapter, in the light of results obtained, the findings from the experiments on Silivri Abadkon, (2012), Erksak Sasitharan, (1989), and six different Anatolian sands Erzin, (2004) are examined. Fitting parameters for the empirical equation obtained as a result of triaxial compression tests were investigated with respect to soil properties.

5.1. Effect of Soil Properties on Peak Dilatancy Angle-Shear Strain at Failure Relationships

Results from the triaxial compression tests on 8 different sands proved that there is a considerable relationship between peak dilatancy angle and their shear strain responses recorded at failure. A natural logarithmic trend was recorded as below:

$$y = -\alpha ln\,(x) + \beta \tag{5.1}$$

where α, β represents fitting parameters and the empirical equation was obtained based on the trend above:

$$\varepsilon_q = e^{\frac{\psi p - \beta}{-\alpha}} \tag{5.2}$$

In order to investigate the influences of soil properties on fitting parameters, data from Abadkon (2012), Sasitharan (1989), and Erzin (2004) studies were examined as below:

Table 5.1. Properties of the Sands Investigated in This Study.

Specimen	G_s	e_{max}	e_{min}	D_{10} (mm)	D_{30} (mm)	D_{60} (mm)	D_{50} (mm)	C_c	C_u	α	β
A*	2.64	0.651	0.4	0.2	0.59	1.16	0.9	1.5	5.8	11.39	29.84
B*	2.62	0.863	0.501	0.53	0.84	1.19	1.13	1.12	2.24	14.19	31.18
C*	2.68	0.613	0.411	0.23	0.39	0.8	0.6	0.83	3.48	10.18	24.01
D*	2.64	0.797	0.584	0.33	0.39	0.41	0.31	1.12	1.24	6.86	24.44
E*	2.7	0.813	0.559	0.21	0.29	0.37	0.22	1.08	1.76	11.03	27.91
F*	2.7	0.818	0.538	0.21	0.33	0.46	0.3	1.13	2.19	9.65	26.9
Erksak Sand	2.66	0.775	0.525	0.21	0.29	0.4	0.34	1	1.9	8.49	21.67
Silivri Sand	2.67	0.96	0.56	0.184	0.325	0.397	0.365	1.45	2.16	9.08	24.13

Specimens of Anatolian Sands from different regions as shown in Table 5.1

Then following figures were drawn according to the soil properties obtained from related studies and fitting parameters of ψ_p - ε_q functions for each sands listed in Table 5.1:

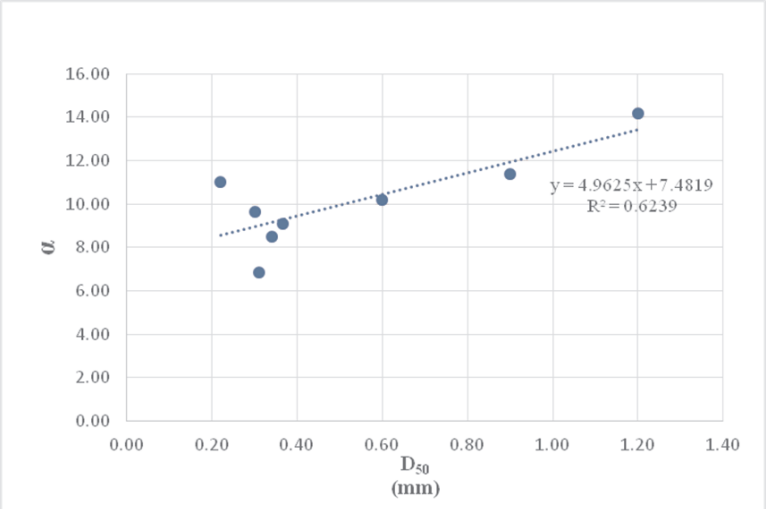


Figure 5.1. Variation of α With Median Grain Size, D_{50}.

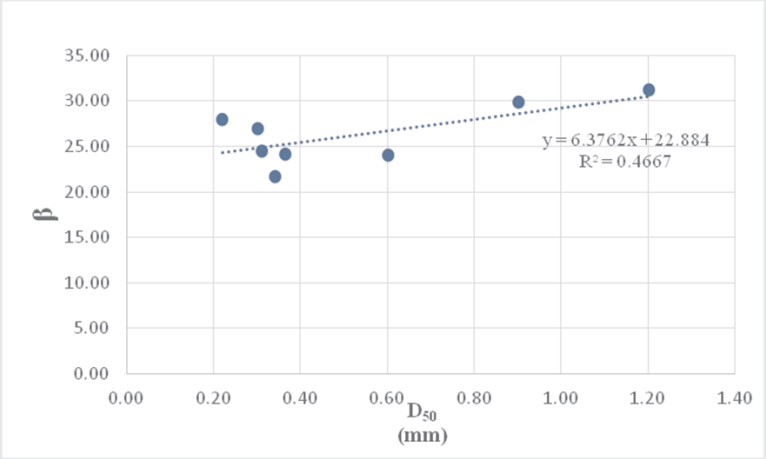


Figure 5.2. Variation of β With Median Grain Size, D_{50}.

According to the results illustrated in Figure 5.1 and Figure 5.2, fitting parameters, α and β have correlations with median grain sizes. However, when examining the fitting parameters with other soil properties such as specific gravity, coefficient of curvature, coefficient of uniformity, no correlation was recorded. For parameter α, the function of the linear trend-line was defined with a coefficient of determination value, R^2, of 0.6239 as below:

$$y = 4.9625x + 7.4819 \tag{5.3}$$

$$\alpha = 4.9625D_{50} + 7.4819 \tag{5.4}$$

In Figure 5.2, the function of the linear trend-line, defining the correlation between the fitting parameter β and median grain size D_{50}, was determined with a coefficient of determination value of 0.4667 as below:

$$y = 6.3762x + 22.884 \tag{5.5}$$

$$\beta = 6.3762D_{50} + 22.884 \tag{5.6}$$

Thus, the empirical equation generated as a result of studies on different sands can be rearranged as below:

$$\varepsilon_q = e^{\frac{\psi_p - 6.38D_{50} - 22.88}{-4.96D_{50} - 7.48}} \tag{5.7}$$

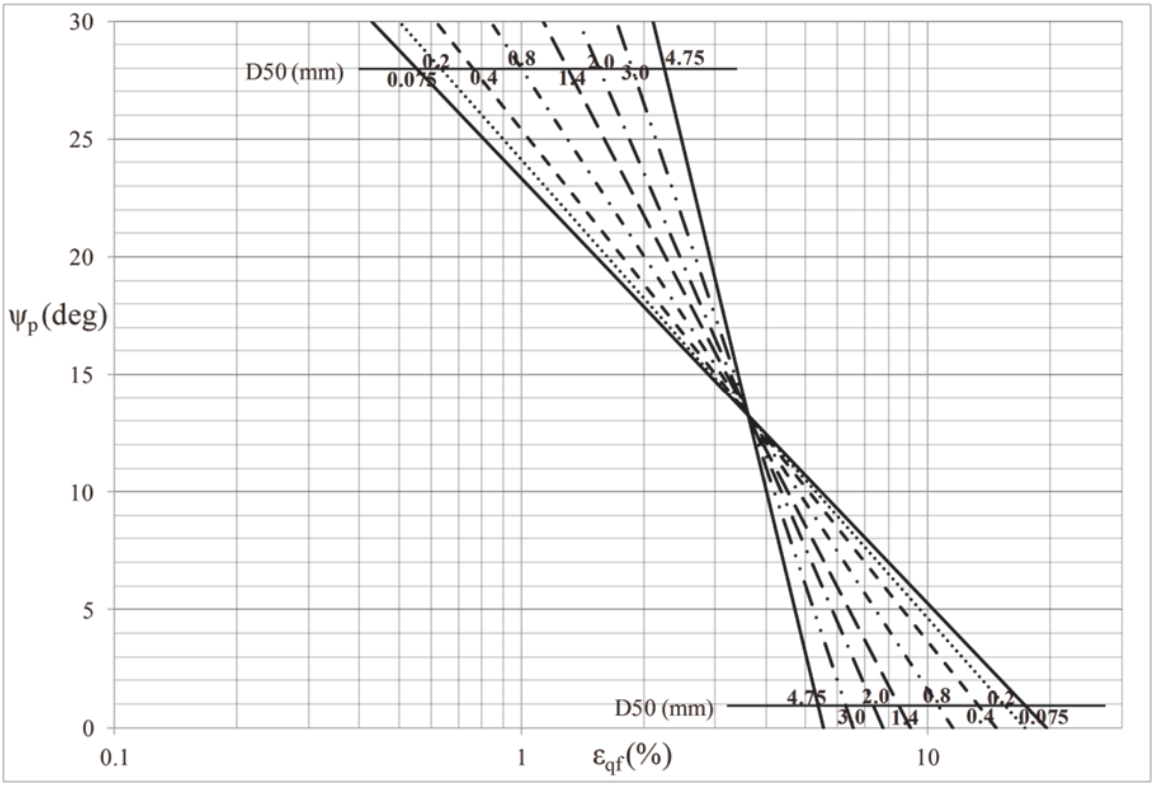


Figure 5.3. Variation of Shear Strain at Failure With Peak Dilatancy Angle and Median Grain Size.

This equation is used to plot the relationship between ψ_p and ε_{q-f} which is shown in Figure 5.3.

Figure 5.3 illustrates the relationship between shear strain at failure and peak dilatancy angle depending on median grain size. Two rulers are used to plot ψ_p - ε_{q-f} relationships by interpolation based on the median grain size, D_{50}.

5.2. Effect OCR on Peak Dilatancy Angle-Shear Strain at Failure Relationship

As the results obtained from the experiments of Abadkon (2012) are grouped in terms of OCR, following peak dilatancy angle-shear strain at failure responses were obtained:

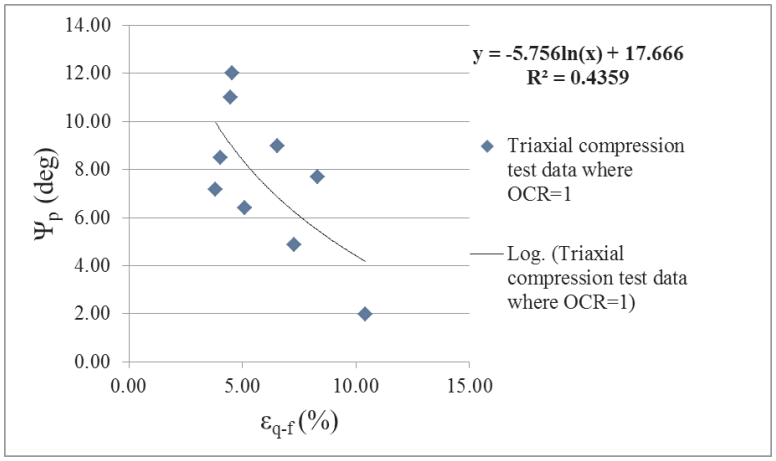


Figure 5.4. Peak Dilatancy Angle-Shear Strain at Failure Response in Case of OCR=1.

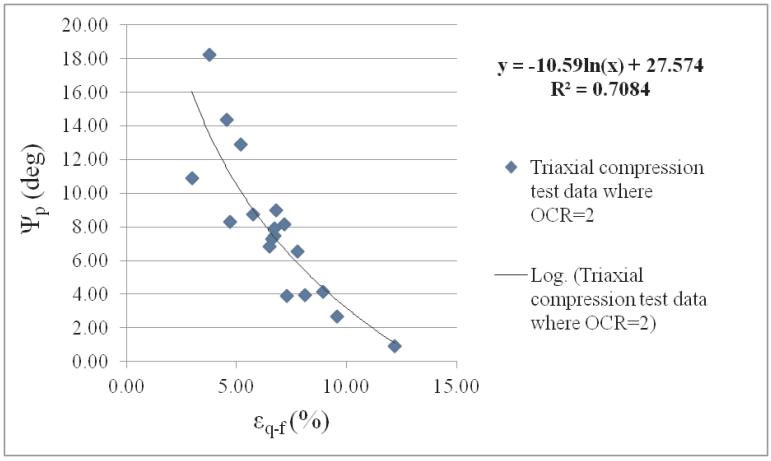


Figure 5.5. Peak Dilatancy Angle-Shear Strain at Failure Response in Case of OCR=2.

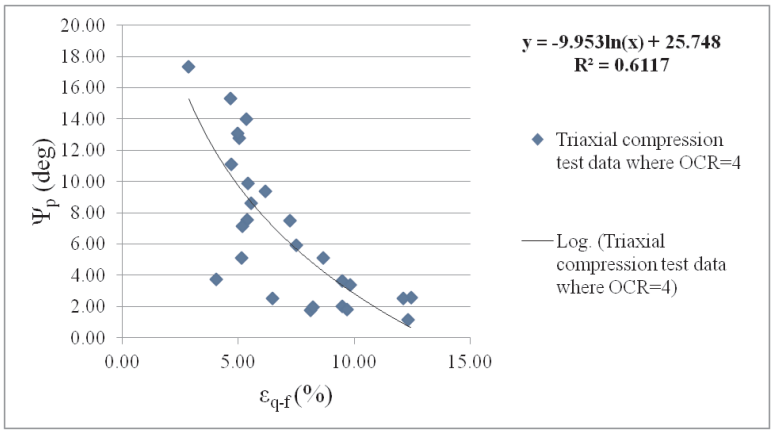


Figure 5.6. Peak Dilatancy Angle-Shear Strain at Failure Response in Case of OCR=4.

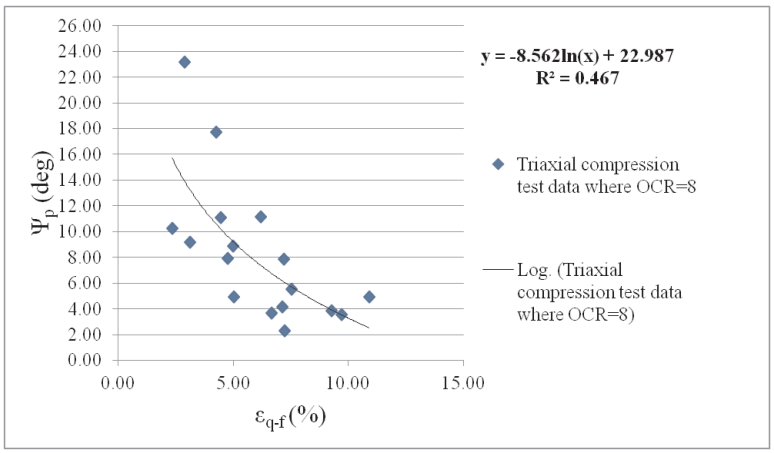


Figure 5.7. Peak Dilatancy Angle-Shear Strain at Failure Response in Case of OCR=8.

In Figure 5.4, variation of peak dilatancy angle with shear strain at failure is shown under the condition in which overconsolidation ratio equals to 1. In the same manner, in Figure 5.5, Figure 5.6, and Figure 5.7 the variations are drawn for the conditions corresponding 2, 4 and 8 respectively. And also the trend-lines fitting the plots for different OCR cases are shown below: For OCR=1,

$$y = -5.756ln(x) + 17.666 \tag{5.8}$$

For OCR=2,

$$y = -10.59ln(x) + 27.574 \tag{5.9}$$

For OCR=4,

$$y = -9.953ln(x) + 25.748 \tag{5.10}$$

For OCR=8,

$$y = -8.562ln(x) + 22.987 \tag{5.11}$$

According to the trend-line functions determined within different OCR cases, it is observed that there was not a significant difference due to variation of OCR except the case of where the OCR equals to 1.

5.3. Implementation of this Method to Design

Most of the engineers may make their choices as selecting the critical state friction angle as the design friction angle in order to be on the safe side. However, in some cases, choosing the critical state friction angle, ϕ'_c, for design friction angle leads to overconservative designs. The results show that engineers designing geotechnical structures and applications can make use of the relationship between peak dilatancy angle and strain at failure in order to make a decision whether to use peak friction angle or critical state friction angle for projects.

The alternative way for selecting design friction angle, "strain-based", is directly related to the deformation limits within the scope of the project. The idea is that possible magnitudes of shear strain in the soil body when the limits of allowable structural deformations are reached are determined by modelling the geotechnical system numerically. After that, magnitude of maximum shear strain value obtained from numerical

analysis is compared with the shear strain at failure value obtained by using graph in Figure 5.3 or the related equation

$$\varepsilon_q = e^{\frac{\psi_p - 6.38D_{50} - 22.88}{-4.96D_{50} - 7.48}} \tag{5.12}$$

Step-by-step implementation of the method is given below:

i) To determine peak dilatancy angle, ψ_p, the equation proposed by Çinicioğlu *et al.*, (2013) can be used since it defines peak dilatancy angle in terms of p'$_i$ and I_D, which is quite easily determined by in-situ tests and laboratory tests, as shown below:

$$tan\psi_p = \alpha_\psi \left(\frac{p'_i}{p_a}\right) + m_\psi I_D \tag{5.13}$$

where α_ψ and m_ψ are unit-independent fitting parameters, I_D is relative density index, ψ_p is peak dilatancy angle (Çinicioğlu *et al.*, 2013). Also, p'_i represents pre-shear mean effective stress where p_a stands for standard atmospheric pressure at sea level. Sieve analysis test, which is a common and quite easy test as well, leads to obtain D_{50} value for the shear strain at failure equation.

ii) D_{50}, median grain size value, which can be obtained by a sieve analysis and calculated ψ_p value are inserted to Equation 5.7 to calculate the shear strain value at failure state of soil. Another way to determine the shear strain value at failure with the knowledge of D_{50} and ψ_p is using the graph (shown in Figure 5.3) which is a product of Equation 5.7.

iii) Then the planned structure is modeled numerically, possibly using a FEM software for applying prescribed displacements. Analyzing the model shows the soil's shear strain response to the specified deformation limit that is defined as prescribed deformation.

Thus the decision of design friction angle can be made by comparing the maximum shear strain obtained from the numerical analysis with the shear strain at failure obtained from Figure 5.3. Even if the maximum shear strain at a single location within the numerical result is greater or equal to ε_{q-f}, then that means ϕ'_c should be used in design. Since evolution of the shear band is a progressive mechanism, having ε_{q-f} even at a singular location signals the formation of a failure surface. Therefore, it is proposed that a certain value of strain based factor of safety should be applied. How that strain-based factor of safety is designed is a topic for future research. However, if maximum shear strain is clearly less than ε_{q-f}, then ϕ'_c can be used in design.

5.3.1. Example 1: Strain-Based Selection of Design Friction Angle According to Results of a FEM Software

A simple model was created in Plaxis to practice the alternative way suggested by this study for selection of design friction angle. A simple footing with a width of 5 m and a thickness of 0.5 m was modeled. The soil modeled under the footing was defined with parameters that are same with Silivri sand of which CD triaxial test data were already examined within this study. For peak dilatancy angle, Equation 2.39 which is dependent on mean effective stress and relative density was used and the peak dilatancy angle was calculated as 10^o. For peak friction angle of soil modeled in Plaxis, the equation proposed by Bishop (1972) was used:

$$\phi'_p = \phi'_c + r\psi_p \tag{5.14}$$

According to the line-fitting parameter, r, and critical state friction angle, ϕ'_c, values for Silivri sand obtained from the literature, the design friction angle was calculated as 38^o which corresponded to soil's maximum friction angle. A prescribed vertical deformation of 0.1 m was defined as a deformation limit since the aim was to see the levels of shear strains and make a decision if it is safe to choose maximum friction angle of soil.

Table 5.2. Properties of Akpinar and Silivri Sands (Çinicioğlu and Abadkon, 2014).

Sand	e_{max}	e_{min}	D_{50} (mm)	C_u	α_ψ	m_ψ	r	ϕ'_c	I_D
Akpinar	0.87	0.52	0.27	1.23	-0.066	0.64	0.39	33.8	0.8
Silivri Sand	0.96	0.56	0.37	2.16	-0.06	0.35	0.46	33	0.65

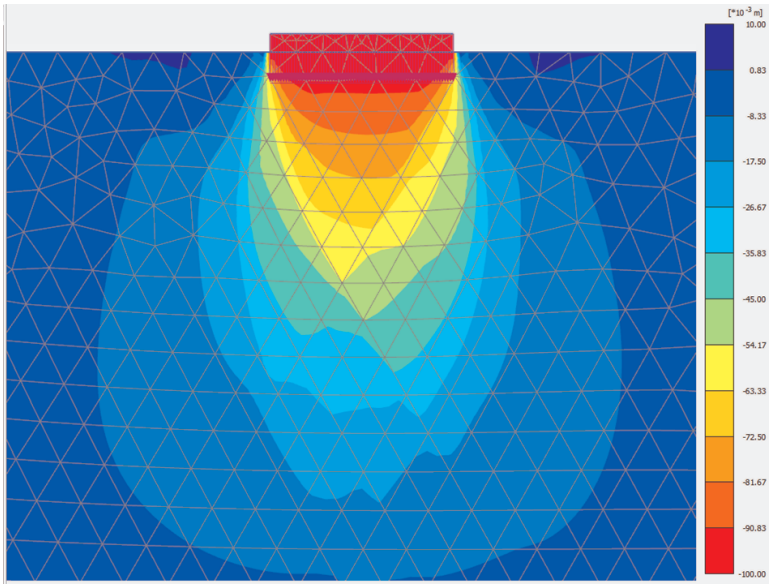


Figure 5.8. Total Displacements in y Direction as a Result of 0.1 M Vertical Displacement of the Structure.

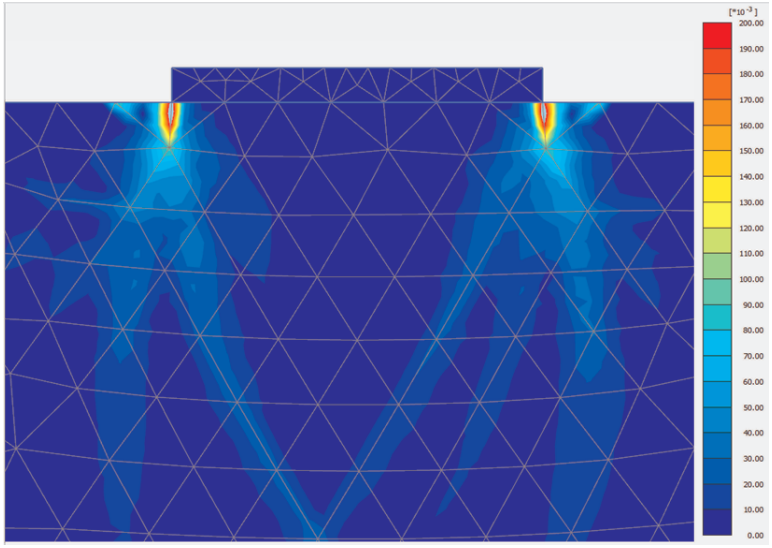


Figure 5.9. Total Shear Strains as a Result of 0.1 M Vertical Displacement of the Structure.

According to the results demonstrated in Figure 5.8 and Figure 5.9, a displacement of 0.1 m triggers shear strains at levels of 4%-5% within the soil. Those values observed by focusing on bending regions concluding the regions right at the wedge of the footing. Hence the shear strain value at failure can be found by the proposed equation and compared with the value obtained by the FEM software:

$$\varepsilon_q = e^{\frac{\psi_p - 6.38D_{50} - 22.88}{-4.96D_{50} - 7.48}} \tag{5.15}$$

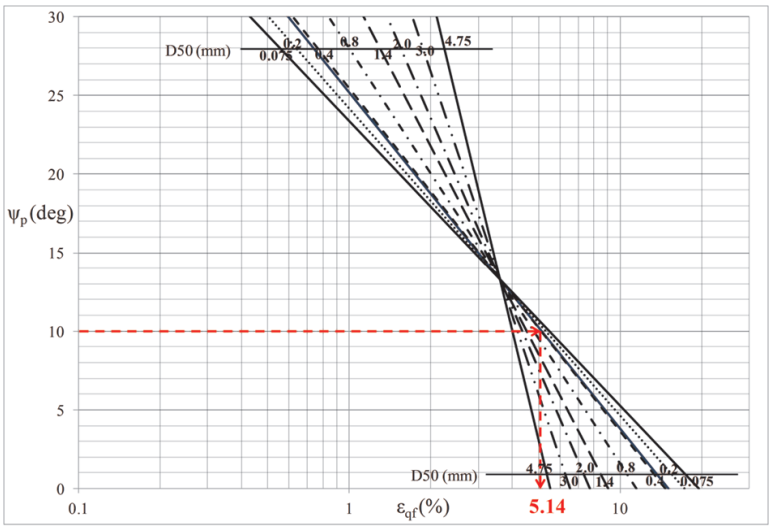


Figure 5.10. Determining the Shear Strain at Failure Value of Silivri Sand With a D_{50} Value of 0.365 by the Proposed Method.

$$\varepsilon_q = 5.14\% > 5\% \tag{5.16}$$

It can be observed that the soil beneath the footing will almost reach the failure strain levels due to the structure's deformation limit of 0.1 m, therefore critical state friction angle of the soil can be selected as a design friction angle in this case. When a prescribed vertical displacement of 2 cm was applied to the same model, the below results were obtained:

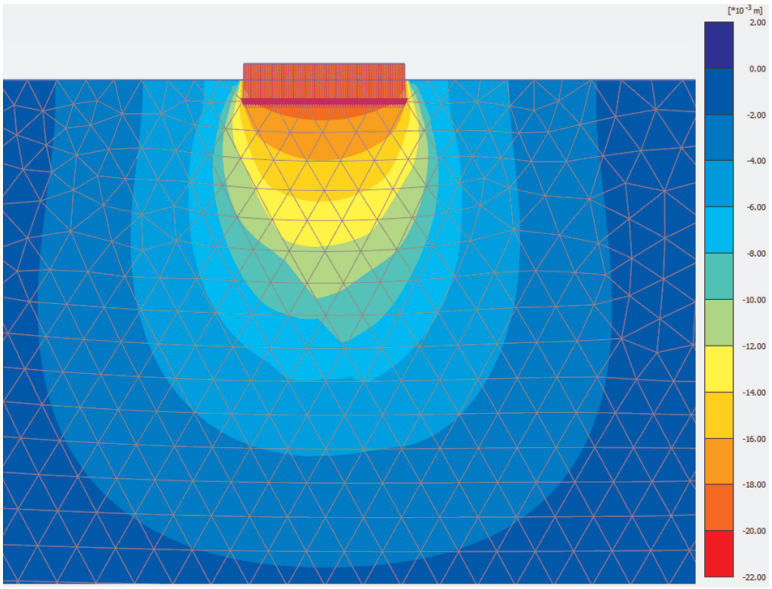


Figure 5.11. Total Displacements in y Direction as a Result of 2 cm Vertical Displacement of the Structure.

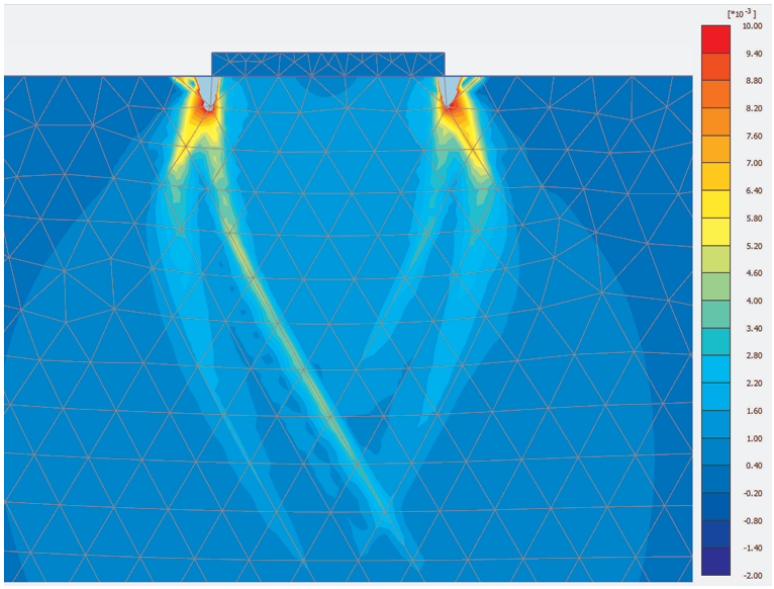


Figure 5.12. Total Shear Strains as a Result of 2cm Vertical Displacement of the Structure.

Based on the results shown in Figure 5.12, a displacement of 2 cm triggers shear strains at levels of 0.8% - 1% within the soil. These values of shear strains that are possible to occur are rather less than the shear strain value at failure calculated as 5.14 by the proposed equation. Therefore, the peak friction angle can be used as the design

friction angle in case of 2 cm structural deformation limit.

5.3.2. Example 2: Strain-Based Selection of Design Friction Angle According to Results of Retaining Wall Physical Model Experiments

A. Altunbas, B. Soltanbeigi, A.T. Gezgin and O. Çinicioğlu (2014) have conducted a physical model study on a 1 g small scale retaining wall model with a purpose of investigating the influence of soil density on the failure surface geometry.

The 1g model consists of a testing box, retaining wall, sand pluviation system, storage tank, crane and software as shown in Figure 5.13. Experiments were conducted in a testing box that is 140 cm long, 60 cm deep, and 50 cm wide. Sides of the testing box are plexiglass allowing the observation and photographing of the soil deformations during testing. Photographs of the backfill at different stages of wall deformation can later be analyzed using Particle Image Velocimetry (PIV) to identify the geometry of failure surfaces.



Figure 5.13. Experimental Set-Up.

The analysis method employed in this study, often introduced as Particle Image Velocimetry (PIV) or Digital Image Correlation (DIC), is a digital image-based surface displacement measurement technique that examines the difference between a reference image and a sequence of deformed images. PIV method is very suitable for

geotechnical investigations of sands, since sands have their own textures in the form of different-colored grains, and due to the light and shadow formed between adjacent grains when illuminated. The GeoPIV algorithm searches for a specified zone of a deformed image that has maximum similarity to the patch's signature in the initial image. The difference between the target patch, measured in pixels, and the reference patch is visualized by the displacement vector (White et al 2003). Both volumetric and shear strains are obtained in this method.

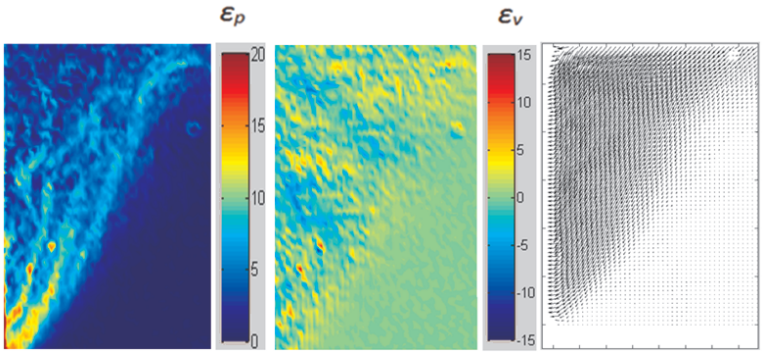


Figure 5.14. Typical Results of PIV Method a) Shear Strain b) Volumetric Strain c) Displacement Vector Field.

One of the outputs of the physical model study, related with this thesis study, was that shear strain values could be measured at different horizontal displacement of retaining wall model by means of (PIV).

Results of physical model experiments conducted with Akpinar sand show that horizontal displacements of 1.5 mm, 2.25 mm, 3 mm correspond to shear strain values of 5%, 18%, and 60% respectively at shear band of the backfill (Figure 5.15). In the light of the data, design friction angle can be decided through the alternative way proposed by this study. Soil properties of Akpinar sand is given in Table 5.3.1 for calculations. The equation proposed by Çinicioğlu et al. (2013) is used to calculate peak friction angle:

$$tan\psi_p = \alpha_\psi \left(\frac{p'_i}{p_a}\right) + m_\psi I_D \tag{5.17}$$

By neglecting the p_i' as the depth of the soil in the physical model is relatively small;

$$tan\psi_p = m_\psi I_D \tag{5.18}$$

$$tan\psi_p = 0.64 \times 0.8 \tag{5.19}$$

$$\psi_p = 27^o \tag{5.20}$$

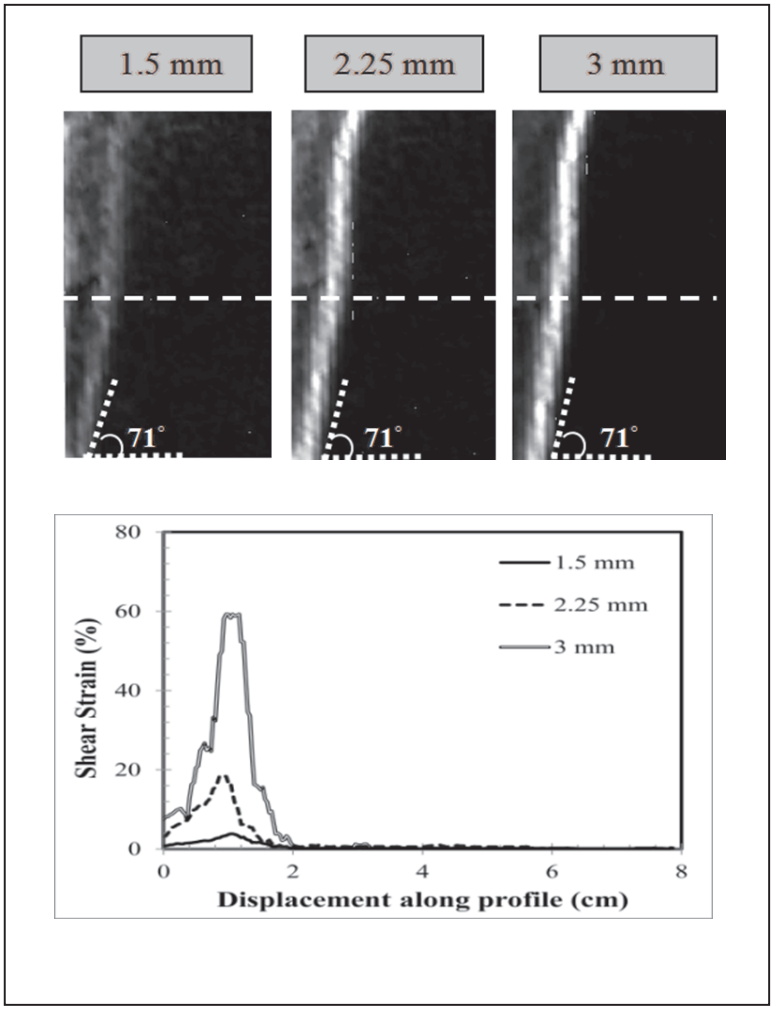


Figure 5.15. Shear Band Formation with Respect to Wall Movement a) Strain Maps for Three Different Stages of Test 1.5, 2.25 and 3 mm b) Intensity Profile of Shear Band on the Proposed Cross-Section (Altunbas *et al.*,2014).

According to the equation proposed by this study, shear strain at failure for Akpinar sand is calculated as;

$$\varepsilon_q = e^{\frac{\psi_p - 6.38D_{50} - 22.88}{-4.96D_{50} - 7.48}} \tag{5.21}$$

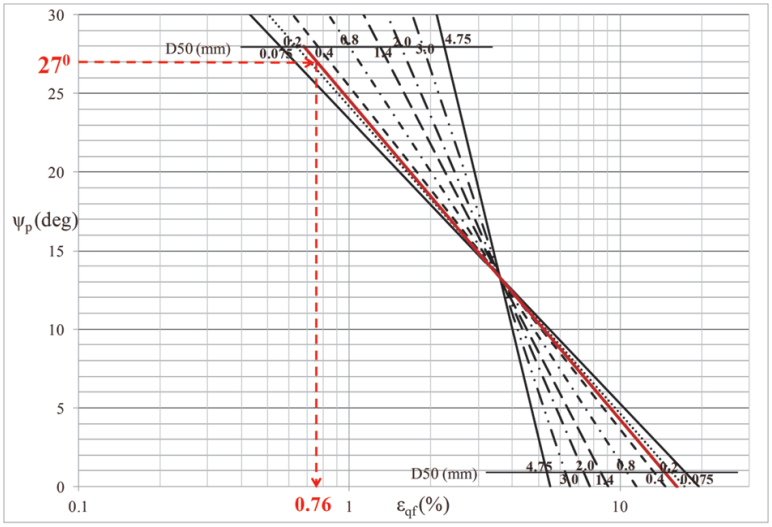


Figure 5.16. Determining the Shear Strain at Failure Value of Akpinar Sand with a D_{50} value of 0.365 by the Proposed Method.

- $\varepsilon_q = 0.76\% < 60\%$ (for the horizontal displacement of 3 mm)
- $\varepsilon_q = 0.76\% < 18\%$ (for the horizontal displacement of 2.25 mm)
- $\varepsilon_q = 0.76\% < 5\%$ (for the horizontal displacement of 1.5 mm)

As the shear strain value at failure state is calculated as 0.51% which is less than the shear strain values corresponding deformations of 3 mm, 2.25 mm, and 1.5 mm according to the physical model experiments, design friction angle should be selected as critical state friction angle of the soil which is 33.8^o.

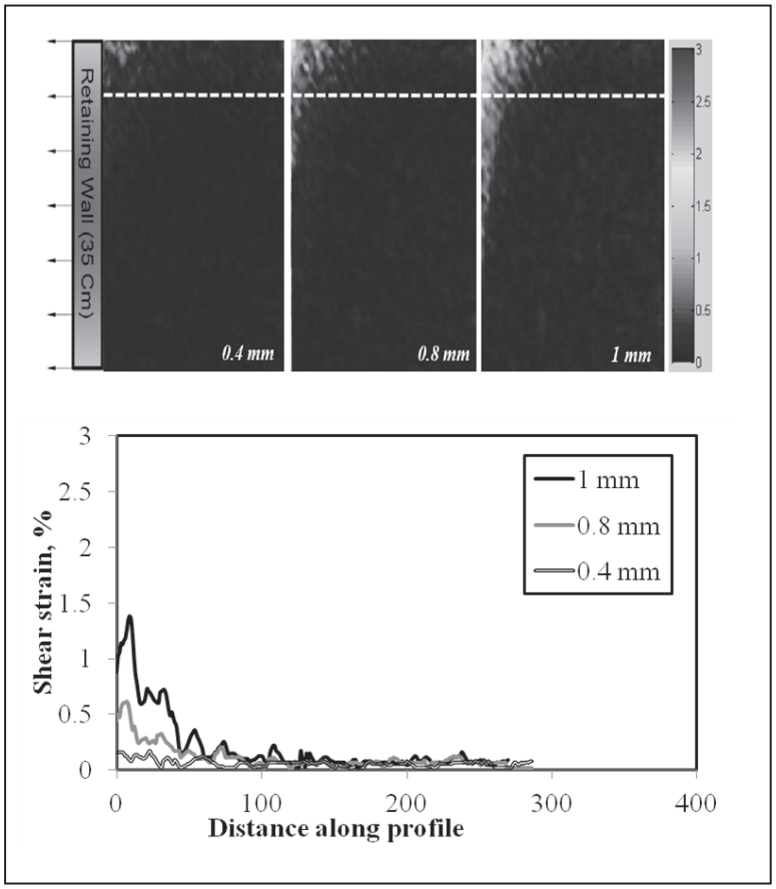


Figure 5.17. Shear Band Formations With Respect to Lesser Diplacements.

In Figure 5.17, it can be observed that horizontal displacements of 1 mm, 0.8 mm, 0.4 mm lead shear strain values of 1.4%, 0.7%, and 0.25% respectively. Comparing the shear strain values obtained from the physical retaining wall model tests with the value obtained as 0.76 by the proposed equation, indicates that use of peak friction angle as design friction angle for a retaining wall backfilled with Akpinar sand can be appropriate where the maximum horizontal displacement limit for the wall is around 0.8 mm. PIV results (Figure 5.17) clearly show that shear plane starts to emerge at wall translations that are equal to or higher than 0.8mm. This corresponds to displacement to wall height of 0.8/350=0.0023. Higher displacements cause the friction angle to drop to residual values.

6. CONCLUSION

The goal of this study is to define a method that would aid the design engineers in the selection of appropriate design soil friction angles. For this purpose, data from 146 CD triaxial tests which were conducted on Silivri, Erksak and 6 different Anatolian sands were examined. The results revealed an emprical relationship between peak dilatancy angle and shear strain at failure state. The reason for selecting peak friction angle as the soil parameter for estimating the magnitude of shear strain at failure is the inherent link between peak dilatancy and failure; peak dilatancy angle is always measured at the instance of failure. Moreover, unlike the friction angle, dilatancy angle is both a deformation and strength parameter. Minimum value of dilatancy angle is zero which makes it a useful benchmark parameter, whereas minimum value of friction angle is the critical state friction angle. Thus, it is not possible to propose a universal link between peak friction angle and failure shear strain. Moreover, it has been noted that the ψ_p-ε_{q-f} relationship is directly dependent on the mean grain diameter for the considered soil. This is expected since the necessary amount of deformation to overcome particle interlocking depends on the average size of grain diameters. Accordingly, influences of D_{50} on obtained ψ_p-ε_{q-f} relationships are quantified and a design chart is developed. This chart enables the researcher to identify the possible magnitude of failure shear strain for a sample of the considered sand using knowledge of p'_i, I_D, and D_{50}. Based on these findings, a step-by-step method for assessing the appropriate design friction angle for sands is proposed. This step-by-step method is presented with an example and its validity is evaluated using the results of a physical retaining wall model study. For this purpose, shear strains within the model backfill that correspond to different wall translation magnitudes are obtained by using Particle Image Velocimetry (PIV). Their values are compared with the ε_{q-f} obtained from the proposed relationship. It is shown that failure plane does not emerge before ε_{q-f} value is reached within the backfill. Most significant outcomes of this study can be summarized as follows:

i) An empirical semi-logarithmic relationship is defined between peak dilatancy angles (ψ_p) and shear strains at failure (ε_{q-f}) for cohesionless soils.

ii) It is shown that ψ_p-ε_{q-f} relationships are dependent on the median grain sizes, D_{50}, of sands.

iii) ψ_p-ε_{q-f} relationships are not affected by overconsolidation ratio (OCR)

iv) A new empirical equation in order to calculate shear strain, ε_q, at failure state in terms of peak dilatancy angle, ψ_p, and median grain size, D_{50}, is proposed. And a design chart as a product of this equation is developed.

v) A step-by-step method for estimating the appropriate design friction angle is proposed. Proposed equations and method are verified using physical model tests.

REFERENCES

Abadkon, A., 2012, "Strength and Dilatancy of Anisotropic Cohesionless Soils", Ph.D. Dissertation, Boğazici University.

American Society for Testing and Materials, 2006, "Standard Test Methods for Maximum Index Density and Unit Weight of Soils Using a Vibratory Table", *ASTM Standards: D4253* .

American Society for Testing and Materials, 2006, "Standard Test Methods for Minimum Index Density and Unit Weight of Soils and Calculation of Relative Density", *ASTM Standards: D4254*.

American Society for Testing and Materials, 2011, "Standard Test Method for Consolidated Drained Triaxial Compression Test for Soils", *ASTM Standards D7181*.

American Society for Testing and Materials, 2006, "Standard Specification for Standard Sand", *ASTM Standards C778*.

Bishop, A.W., 1950, "Discussion to 'Measurement of the shear strength of soils' by Skempton and Bishop", *Geotechnique*, Vol. 2, No. 1, pp. 113-116.

Bolton, M.D., 1986, "Strength and Dilatancy of Sands", *Geotechnique*, Vol. 36, No. 1, pp. 65-78.

Çinicioğlu, O., A., Abadkon, A., Altunbas and M., Abzal, 2013, "Variation of friction angle and dilatancy for anisotropic coheisonless soils", *Paris: Proceedings, 18th International Conference on Soil Mechanics and Geotechnical Engineering*.

Chakraborty, T. and R. Salgado, 2010, "Dilatancy and Shear Strength of Sand at Low Confining Pressures", *Journal of Geotechnical and Geoenvironmental Engineering*, Vol. 136, No. 3, pp. 527-532.

Craig, R.F., *Soil Mechanics*, Spon Press, London and New York, 2004.

Erzin, Y., 2004, "Strength of Different Anatolian Sands in Wedge Shear, Triaxial Shear, and Shear Box Tests", Ph.D. Dissertation, The Middle East Technical University.

Houlsby, G.T., 1991, "How the Dilatancy of Soils Affects Their Behaviour", *10th European Conference on Soil Mechanics and Foundation Engineering*, Report Number OUEL 1888/91.

Kramer, S.L., *Geotechnical Earthquake Engineering*, Prentice-Hall, Inc., Upper Saddle River, NJ, USA, 1996.

Mair, R.J. and D.M., Wood, 1987. "Pressuremeter testing methods and interpretation", *CIRIA Ground Engineering Report: In-situ Testing.* Butterworths, London.

Powrie, W., *Soil Mechanics: concepts and applications 2nd edition*, Spon Press, London and New York, 2004.

Rowe, P.W., 1969, "The Relation between the Shear Strength of Sands in Triaxial Compression, Plane Strain and Direct Shear", *Geotechnique*, Vol. 19, No. 1, pp. 75-86.

Rowe, P.W., 1962, "The Stress-Dilatancy Relation for Static Equilibrium of an Assembly of Particles in Contact", *Proceeding of the Royal Society of London. Series A, Mathematical and Physical Sciences*, Vol. 269, No. 1339, pp. 500-527.

Santamarina, J.C. and G.C., Cho, "Determination of Critical State Parameters in Sandy Soils-Simple Procedure", *Geotechnical Testing Journal*, GTJODJ, Vol. 24, No. 2, June 2001, pp. 185-192.

Sasitharan, S., 1989, "Stress Path Dependency of Dilatancy and Stress-Strain Response of Sand", M.Sc Dissertation, The University of British Columbia.

Schanz, T., and P.A., Vermeer, 1996, "Angle of Friction and Dilatancy of Sand",

Geotechnique, Vol. 46, No. 1, pp.145-151.

Triaxial User's Manual, Geocomp Corporation, 2007.

Vaid, Y.P., and S., Sasitharan, 1992, "The Strength and Dilatancy of Sand", *Canadian Geotechnical Journal*, Vol. 29, pp. 522-526.

Wood, D.M., Geotechnical Modelling, Spon Press, London, UK, 2004.

White, D.J., W.A., Take and M.D., Bolton, 2003, "Soil deformation measurements using particle image velocimetry PIV and photogrammetry", *Geotechnique*, Vol. 53, pp. 619-631.